

Merging black holes with Cauchy-characteristic matching: Computing late-time tails

Sizheng Ma ^{1,*} Mark A. Scheel ² Jordan Moxon ² Kyle C. Nelli ² Nils Deppe ^{3,4,5} Lawrence E. Kidder ⁵ William Thrope ⁵ and Nils L. Vu ²

¹*Perimeter Institute for Theoretical Physics, Waterloo, ON N2L2Y5, Canada*

²*TAPIR 350-17, California Institute of Technology, 1200 E California Boulevard, Pasadena, CA 91125, USA*

³*Laboratory for Elementary Particle Physics, Cornell University, Ithaca, New York 14853, USA*

⁴*Department of Physics, Cornell University, Ithaca, New York 14853, USA*

⁵*Cornell Center for Astrophysics and Planetary Science, Cornell University, Ithaca, New York 14853, USA*

(Dated: July 3, 2025)

Cauchy-characteristic matching (CCM) is a numerical-relativity technique that solves Einstein’s equations on an effectively infinite computational domain, thereby eliminating systematic errors associated with artificial boundary conditions. Whether CCM can robustly handle fully nonlinear, dynamical spacetimes, such as binary black hole (BBH) mergers, has remained an open question. In this work, we provide a positive answer by presenting nine successful CCM simulations of BBHs; and demonstrate a key application of this method: computing late-time tails. Our results pave the path for systematic studies of late-time tails in BBH systems, and for producing highly accurate waveforms essential to next-generation gravitational-wave detectors.

I. INTRODUCTION

The detection of gravitational waves (GWs) by the LIGO, Virgo, and KAGRA collaboration [1–7] has revolutionized our ability to explore the strong-field regime of gravity in compact binary systems. A key ingredient in GW astronomy is the accurate modeling of GW signals from binary black hole (BBH) mergers — the dominant sources in current observations — to reliably extract them from detector noise.

To date, numerical relativity (NR) remains the only *ab initio* method capable of computing the full nonlinear waveforms from BBHs. In particular, NR simulations are used to calibrate effective-one-body models [8–12] and to construct surrogate waveforms [13–16], both of which have become essential tools in LIGO-Virgo-KAGRA data analysis [1–4, 17–23]. However, meeting the stringent requirements of next-generation GW detectors will require NR accuracy to improve by an order of magnitude [24]. Systematic errors in NR waveforms — if left unaddressed — could lead to false alarms or deviations from general relativity. Therefore, reducing or eliminating these systematics is a critical priority for future GW astronomy.

The most commonly used approach in NR is the Cauchy formulation, in which spacetime is foliated into spacelike hypersurfaces and Einstein’s equations are decomposed into evolution and constraint sets via the 3+1 decomposition (see, e.g., [25]). Since the Cauchy formulation is restricted to a finite computational domain, an artificial outer boundary must be introduced, along with appropriate boundary conditions. These conditions typically approximate, rather than reproduce exactly, the behavior of gravitational fields that extend to infinity and can thus become a significant source of systematic error, e.g., see [26, 27]. To overcome this issue, it is desirable to develop

NR frameworks that directly incorporate null infinity, where GWs are unambiguously defined.

One promising method is to use hyperboloidal slices [28–34], which are spacelike hypersurfaces that approach future null infinity \mathcal{I}^+ . By introducing a compactified radial coordinate, future null infinity is brought to a finite coordinate distance on the computational domain, thereby removing artificial outer boundaries and allowing GWs to be extracted directly at \mathcal{I}^+ . Another strategy is based on the generalized conformal field equations [35–39], which simultaneously include both past and future null infinities \mathcal{I}^\pm within a unified computational framework. This enables the study of the global structure of spacetime and scattering processes between \mathcal{I}^- and \mathcal{I}^+ [39]. However, current numerical implementations of both approaches are largely limited to single BHs or simple spacetimes (with symmetries), and their extension to fully generic BBH mergers remains a challenge.

A third option to include null infinity is the characteristic formulation [40–47], in which spacetime is foliated by null hypersurfaces that extend to \mathcal{I} . As in the hyperboloidal approach, a compactified radial coordinate maps null infinity to the finite boundary of the computational domain, which in turn enables unambiguous extraction of GWs at \mathcal{I} . However, the characteristic method faces challenges in evolving the near-zone region of BBH spacetimes due to the formation of caustics — regions where neighboring null rays focus and intersect — resulting in coordinate singularities [48–53]. Such singularities undermine the stability and accuracy of the characteristic simulation in highly dynamical or strongly curved regions.

Since the Cauchy and characteristic formulations are naturally complementary, they can be combined to achieve a complete description of gravitational fields. In this hybrid approach, the Cauchy system first evolves the near-zone dynamics and provides metric data on a timelike worldtube, which is then used as input for the characteristic evolution that propagates the data to future null infinity. This two-step method for extracting gravita-

* sma2@perimeterinstitute.ca

tional radiation is known as Cauchy-characteristic evolution (CCE) [40, 42–47, 54–76]. The first CCE simulation of BBH systems was given by Reisswig *et al.* [67], and the method has been applied to studies of memory effects [75, 76]. Despite recent fruitful progress, CCE has a notable limitation: its data flow is strictly one-way. The characteristic evolution depends on the Cauchy data, but not vice versa — meaning the Cauchy simulation must still be run with artificial outer boundary conditions. As a result, while CCE offers a robust and gauge-invariant method for extracting waveforms at \mathcal{I}^+ , it does not eliminate systematic errors introduced by inaccurate Cauchy boundary conditions.

Cauchy-characteristic matching (CCM) [40, 41, 77] is a natural solution to this limitation. Unlike CCE, where the Cauchy and characteristic evolutions are performed sequentially, CCM evolves both systems simultaneously, with each providing *exact* boundary data for the other. The Cauchy evolution supplies interior data to the characteristic domain at the worldtube, while the characteristic system, in turn, provides outer boundary data for the Cauchy evolution. This mutual exchange eliminates the need for artificial boundary conditions entirely and allows for a seamless and self-consistent evolution from the strong-field near zone out to future null infinity.

Despite the conceptual appeal of CCM, its numerical implementation has proven challenging [40]. Early efforts focused on spacetimes with spherical symmetry [78, 79], cylindrical symmetry [80–82], and axial symmetry [83, 84]. In three dimensions, CCM has only been implemented perturbatively [85–87]: the wave zone was not evolved fully nonlinearly with a characteristic code, but instead modeled using linearized perturbations of Schwarzschild spacetime. This approach yielded simulations of 3D Teukolsky waves propagating on a flat background [85], but left unresolved the feasibility of applying CCM to fully nonlinear, dynamical spacetimes like BBH mergers. More critically, it was later pointed out that CCM may be only weakly hyperbolic [40, 88–92], implying that a stable numerical implementation may not exist in general. This concern further cast doubt on the long-term viability of the CCM program¹.

Recently, we developed a fully relativistic algorithm to perform CCM for *any* numerical spacetime [93] (hereafter Paper I). The method is free of approximations and has already demonstrated stability in simulations of simple systems such as single BHs and flat spacetime. In this paper, we apply the same algorithm to BBH mergers and show that CCM is not only feasible in this highly dynamical regime but also yields stable, convergent, and high-accuracy simulations. As discussed in Paper I, a key advantage of CCM is its ability to model backscattering effects, which are closely related to GW tails [94–98]. In what follows, we demonstrate that our CCM framework

can indeed resolve the late-time tails arising from BBH mergers.

This paper is organized as follows. In Sec. II, we briefly summarize the CCM algorithm designed in Paper I. Next in Sec. III, we present nine CCM simulations of BBH mergers, along with late-time tails uncovered through this method. These tails are then analyzed phenomenologically in Sec. IV. Finally, we summarize the results in Sec. V.

Throughout this paper we use Latin indices i, j, k, \dots to denote 3D spatial components and Greek indices μ, ν, \dots for 4D spacetime components. The initial ADM mass of binary systems is denoted by M .

II. SUMMARY OF CCM

In this section, we provide a brief overview of the CCM algorithm developed in Paper I and refer the reader to the paper for more details.

Our Cauchy evolution adopts the Generalized Harmonic (GH) formalism described in [99], which formulates the vacuum Einstein equations as first-order symmetric hyperbolic partial differential equations. This system evolves fifty variables: the metric $g_{\mu\nu}$, its normal-time derivative $\Pi_{\mu\nu} = \alpha^{-1}(\beta^i \partial_i g_{\mu\nu} - \partial_t g_{\mu\nu})$, and spatial derivative $\Phi_{i\mu\nu} = \partial_i g_{\mu\nu}$, where α and β^i are the lapse and shift, respectively.

At the outer boundary of the Cauchy domain, boundary conditions are imposed on forty incoming characteristic fields, including [99, 100]

$$\begin{aligned} u_{\mu\nu}^0 &= g_{\mu\nu}, & u_{i\mu\nu}^2 &= P_i^k \Phi_{k\mu\nu}, \\ u_{\mu\nu}^{1-} &= \Pi_{\mu\nu} - s^i \Phi_{i\mu\nu} - \gamma_2 \psi_{\mu\nu}, \end{aligned} \quad (1)$$

where s^i is the outward unit normal vector of the boundary, $P_i^k = \delta_i^k - s_i s^k$ is the projection operator, and γ_2 is a constraint damping parameter. As noted in [99], the boundary conditions can be divided into three subsets: constraint, physical, and gauge.

In the constraint subset, the normal derivatives of $u_{\mu\nu}^0$, $u_{i\mu\nu}^2$, and four components of $u_{\mu\nu}^{1-}$ are related to incoming constraint modes [see Eq. (59)–(61) in [99]]. Imposing constraint-preserving conditions yields Neumann conditions on these thirty-four variables. Thus, CCM is unnecessary here, as manual constraint injection lacks physical motivation and may cause numerical instability.

The physical subset involves two other components of $u_{\mu\nu}^{1-}$ and encodes information about backscattered GWs. According to Eq. (66) and (67) in [99] and Eq. (2.12) in Paper I, these degrees of freedom are related to the Weyl scalar Ψ_0 , corresponding to the two polarizations of the backscattered radiation. Setting boundary conditions for this subset requires precisely modeling the backscattered waves outside the Cauchy domain, which was achieved in Paper I. Since the two components of $u_{\mu\nu}^{1-}$ are represented on the Cauchy grid with the Cauchy tetrad, careful gauge and tetrad transformations are necessary before matching.

¹ See Sec. V for more discussions.

Table I. List of BBH simulations considered in this work. Here $q \geq 1$ stands for the mass ratio. Each binary is initialized with an orbital angular velocity Ω_{orb} (the transverse velocity relative to the line connecting the two BHs) and a radial velocity \dot{r} . The merger time corresponds to the formation of a common apparent horizon. The remnant Kerr BH has mass M_f and dimensionless spin χ_f . CPU hours are provided for each simulation. Reference systems involve sequential Cauchy and characteristic evolutions, their CPU times are listed in the format (Cauchy)+(characteristic).

| Systems | CCM or Reference | q | $M\Omega_{\text{orb}}$ (10^{-5}) | \dot{r} (10^{-4}) | Initial Separation (M) | Boundary Radius (M) | Merger Time (M) | M_f/M | χ_f | CPU Time (h) |
|----------------|------------------|-----|---|----------------------------|-------------------------------|----------------------------|------------------------|---------|-----------------------|-----------------|
| Head-on | CCM | 1 | 0 | 0 | 110 | 650 | 1323.7 | 0.99712 | 1.1×10^{-9} | 3263.4 |
| | Reference 1 | 1 | 0 | 0 | 110 | 6000 | 1323.7 | 0.99712 | 4.0×10^{-10} | 10211.2+2 |
| | CCM | 2 | 0 | 0 | 110 | 650 | 1323.8 | 0.99752 | 3.7×10^{-9} | 5556.7 |
| | Reference 2 | 2 | 0 | 0 | 110 | 4672 | 1323.8 | 0.99752 | 2.5×10^{-9} | 11297.1+2 |
| | CCM | 4 | 0 | 0 | 110 | 650 | 1323.7 | 0.99830 | 2.1×10^{-9} | 10289.1 |
| | Reference 4 | 4 | 0 | 0 | 110 | 4800 | 1323.8 | 0.99830 | 2.2×10^{-9} | 18770.3+2 |
| Quasi Head-on | CCM | 1 | 8.562 | 0 | 110 | 650 | 1332.9 | 0.99655 | 0.259 | 3128.1 |
| | Reference 1 | 1 | 8.562 | 0 | 110 | 4800 | 1332.9 | 0.99655 | 0.259 | 8974.3+2 |
| | CCM | 1 | 17.123 | 0 | 110 | 650 | 1362.3 | 0.99340 | 0.509 | 3476.1 |
| | Reference 1 | 1 | 17.123 | 0 | 110 | 4669 | 1362.3 | 0.99340 | 0.509 | 8766.5+2 |
| | CCM | 1 | 25.686 | 0 | 110 | 650 | 1422.2 | 0.97602 | 0.715 | 5022.7 |
| | Reference 1 | 1 | 25.686 | 0 | 110 | 4800 | 1422.2 | 0.97602 | 0.715 | 14641.8+2 |
| | CCM | 1 | 29.967 | 0 | 110 | 650 | 1498.8 | 0.94480 | 0.696 | 6775.1 |
| | Reference 1 | 1 | 29.967 | 0 | 110 | 4800 | 1498.8 | 0.94480 | 0.696 | 17556.9+2 |
| Eccentric | CCM | 1 | 58.102 | 0.31 | 90 | 650 | 14781 | 0.95272 | 0.689 | 14318.6 |
| Quasi Circular | CCM | 1 | 1979.005 | 2.6 | 13 | 300 | 2561.8 | 0.95159 | 0.686 | 3178.1 |

We have verified that neglecting these transformations can cause instability in CCM simulations. In Paper I, we developed a general method for handling these transformations in any numerical spacetime.

In the wave zone, a numerical spacetime can be approximated as a perturbed Schwarzschild BH, allowing the use of the Regge-Wheeler-Zerilli (RWZ) formalism to estimate the evolution of Ψ_0 . This approach leads to “higher order boundary conditions” (HOBCs) [101–104] that absorb outgoing multipolar radiation up to a specified angular momentum order L . HOBCs have three major approximations: (1) nonlinear effects are omitted; (2) a truncation order L must be chosen; (3) the RWZ formalism is applied in the BH’s rest frame, usually different from the Cauchy frame. Although Ψ_0 is an invariant at the linear level, it is still represented on the Cauchy grid and thus the angular coordinate mismatch at the boundary between the rest and Cauchy frames can cause mode mixing. Our CCM implementation relaxes these approximations, effectively providing an infinite-order ($L = \infty$) nonlinear boundary condition. When linearized around a Schwarzschild background, the CCM algorithm should reproduce HOBCs.

Finally, the gauge subset determines the remaining four components of $u_{\mu\nu}^1$. It implicitly sets the boundary conditions for the GH gauge [103, 105–107]

$$\square x^\mu = H^\mu, \quad (2)$$

where \square is the d’Alembert operator, and H^μ are freely

specifiable gauge source functions, here chosen as the Damped Harmonic gauge [108]. While this subset controls the dynamics of the Cauchy grids, it *does not* affect GWs [109] once transformed into the Bondi-Sachs frame (modulo BMS transformations [110, 111]), which represents inertial observers at future null infinity. Therefore, for waveform modeling, CCM is not required for this subset.

However, this does not mean that the gauge subset is unimportant in numerical simulations. As noted in [112], poorly chosen gauge boundary conditions can cause an exponential drift of a binary’s center of mass over a long timescale. Although this drift is a gauge effect, it can lead to numerical challenges and increase computational costs. In the following discussions, we mainly adopt the Sommerfeld boundary condition for the subset [106].

To summarize, the primary implementation challenge of CCM is to model backscattered GWs. In strong-gravity regions, it is well known that there is no canonical definition for local physical quantities like gravitational energy. This suggests that CCM could naturally be a cumbersome procedure, requiring the consideration of all dynamical variables. However, the GH formalism simplifies this significantly by providing a framework to isolate the relevant subset of variables. By focusing exclusively on this reduced subset, along with the tricks described in Paper I, CCM becomes computationally manageable.

III. NUMERICAL SIMULATIONS

In this section, we present nine CCM simulations of BBH mergers, with configurations summarized in Table I. Our code setup follows a hybrid approach: we adopt the NR code SpECTRE [113] to handle the characteristic system, while leveraging the more mature code SpEC [114] for the Cauchy evolution. Our design links the SpECTRE characteristic module to SpEC’s executable, enabling SpEC to invoke SpECTRE functions as needed throughout the simulation. Specifically, we adopt SpEC’s time stepper, chosen as the fifth-order Dormand-Prince integrator, to evolve both Cauchy and characteristic variables. The SpECTRE module is used only for evaluating the right-hand sides of the characteristic equations and computing quantities necessary for CCM.

Our CCM system can stably evolve BBH mergers without requiring fine-tuning of constraint damping parameters. We use common values as in other SXS simulations, see Eqs. (53), (54), and Table 2 of [115]. Simulations are run at three resolutions (“Low”, “Medium”, and “High”). The Cauchy resolution is set by specifying numerical error tolerances for the adaptive mesh refinement algorithm [116], while the characteristic resolution is controlled by the number of grid points in angular and radial directions.

The SpEC initial data solver generates Cauchy initial data through the Extended Conformal Thin Sandwich formulation [117–119]. Superposed harmonic-Kerr [120] data is adopted to reduce junk radiation.

While Sec. II E of [47] lists various methods to construct characteristic initial data, it omits details of SpECTRE’s default algorithm, which we summarize in Appendix A.

A. Head-on collisions

We first consider head-on collisions of two nonspinning BHs with various mass ratios. As summarized in Table I, the initial separation is set to $110M$, and the initial boost velocity is 0. The outer boundary and the time-like worldtube for CCM are placed at a radius of $650M$ from the center of mass. In this setup, the Cauchy domain is relatively small, making the interior dynamics in causal contact with the outer boundary within the merger time ($t \sim 1323.7M$). Consequently, the Cauchy boundary conditions impact the evolution.

The black curve in Fig. 1 shows the CCM evolution of the $(\ell = 2, m = 0)$ harmonic of Ψ_4 at future null infinity for the equal-mass system ($q = 1$), computed at the highest resolution. It is compared to the extraction without matching (in blue). We focus on Ψ_4 because its functional form is unaffected by supertranslations, see Eq. (17e) in [121], thus avoiding a constant offset from memory effects². Significant differences are evident at

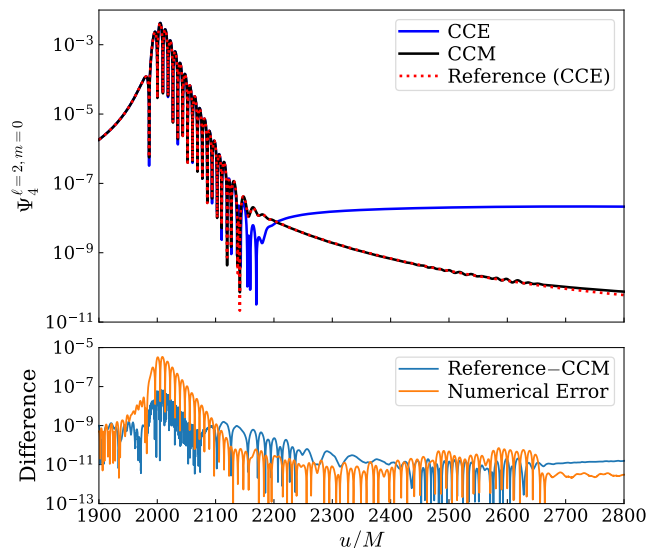


Figure 1. Top panel: $\Psi_4^{\ell=2, m=0}$ emitted from the equal-mass ($q = 1$) head-on BBH collision, simulated using CCE (blue) and CCM (black). The “High” resolution is used. They are compared to a reference system (red), whose outer boundary remains causally disconnected from the binary throughout the simulation. Bottom panel: The difference between the reference and CCM results (blue), along with an estimate of the numerical error (orange) by taking the difference between two adjacent CCM resolutions (“Medium” and “High”).

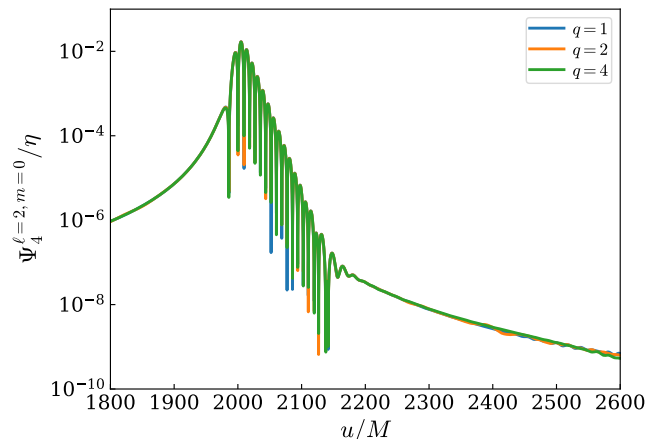


Figure 2. CCM-extracted $\Psi_4^{\ell=2, m=0}$, normalized by the symmetric mass ratio η [Eq. (3)], for the head-on collisions with various mass ratios ($q = 1, 2, 4$; see Table I).

late times. To validate the CCM simulation, we conduct a reference simulation without CCM, whose outer boundary, positioned at $6000M$, remains causally disconnected from the system. This reference result (in red) nearly overlaps the black curve. The lower panel of Fig. 1 shows the difference between the reference and CCM results (in blue), together with an estimate of numerical error obtained by taking the difference between two adjacent CCM resolutions (“Medium” and “High”). The compar-

² In other words, Ψ_4 is expected to vanish after the system settles, making it more convenient to look for late-time tails.

ble differences confirm that CCM accurately converges to the exact infinite domain problem.

To examine the effect of mass ratio q , we normalize $\Psi_4^{\ell=2,m=0}$ by the symmetric mass ratio η :

$$\eta \equiv \frac{m_1 m_2}{(m_1 + m_2)^2} \equiv \frac{q}{(1+q)^2}. \quad (3)$$

As shown in Fig. 2, the normalized Ψ_4 's align remarkably well across different mass ratios, indicating that the overall time evolution scales cleanly with η . In fact, this scaling behavior has been previously observed in the perturbative regime (e.g., [122]); here, we confirm its validity in the fully nonlinear setup.

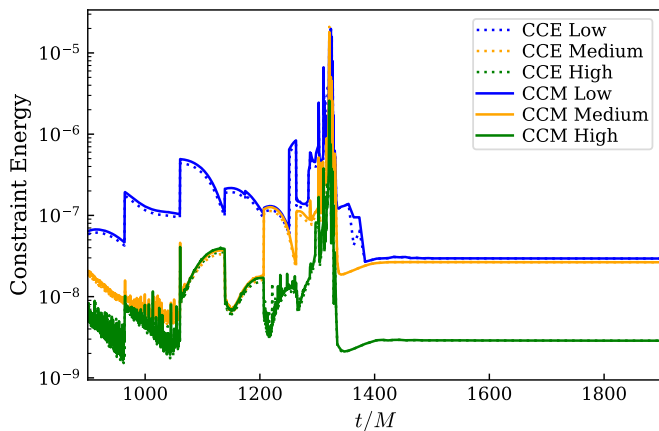


Figure 3. L^2 -norm of the Cauchy GH constraint energy for the equal-mass head-on collision, simulated with CCM (solid curves) and CCE (dashed curves) at three resolutions. The Cauchy time t is used.

Besides waveform comparisons, we also assess the accuracy of our CCM simulations by monitoring constraint violations. A CCM system consists of a Cauchy sector and a characteristic sector, each with its own constraints. For the Cauchy sector, constraints are encoded in the GH constraint energy, as defined in Eq.(53) of [99]. Figure 3 shows its L^2 -norm for the equal-mass system at three resolutions (solid curves). The constraints converge with resolution and become constant once the system settles down. No instabilities are observed. A comparison with a standard Cauchy evolution (without matching but under otherwise identical conditions) shows that CCM does not significantly alter the constraint energy (dotted curves), in agreement with Paper I.

As for the characteristic sector, Einstein's equations and the Bianchi identities link the Weyl scalars $\Psi_{0,1,2,3,4}$ and the strain h at future null infinity. Specifically, the following constraints should vanish in the exact limit (see,

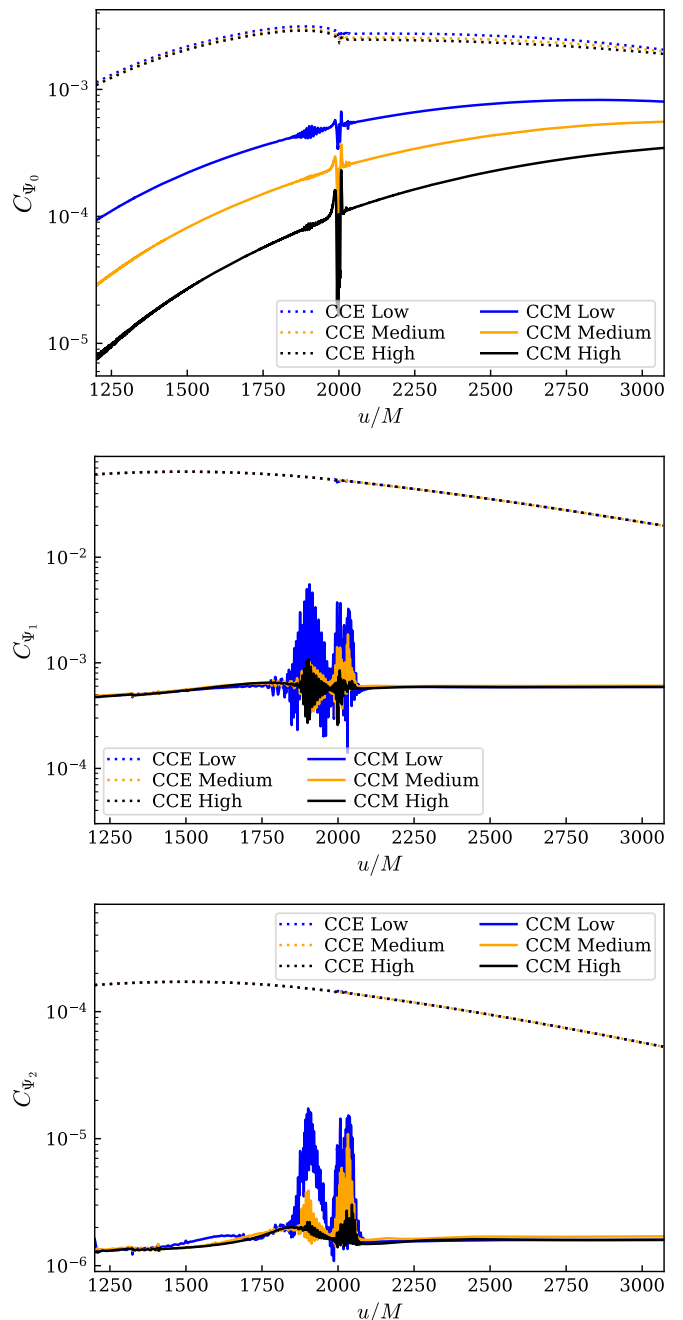


Figure 4. L^2 -norm of C_{Ψ_0} , C_{Ψ_1} , and C_{Ψ_2} , as defined in Eq. (4), for the equal-mass head-on collision, simulated with CCM (solid curves) and CCE (dashed curves) at three resolutions. The retarded time u is used.

e.g., [123, 124]):

$$C_{\Psi_2} \equiv \dot{\Psi}_2 + \frac{1}{2}\bar{\delta}\Psi_3 - \frac{1}{4}\bar{h}\Psi_4, \quad (4a)$$

$$C_{\Psi_1} \equiv \dot{\Psi}_1 + \frac{1}{2}\bar{\delta}\Psi_2 - \frac{1}{2}\bar{h}\Psi_3, \quad (4b)$$

$$C_{\Psi_0} \equiv \dot{\Psi}_0 + \frac{1}{2}\bar{\delta}\Psi_1 - \frac{3}{4}\bar{h}\Psi_2, \quad (4c)$$

where the dot represents the retarded-time derivative, $\bar{\partial}$ denotes the angular derivative, and the bar stands for complex conjugation. Since our characteristic evolution computes those quantities independently, these relations yield nontrivial constraints that can be used to assess the accuracy of our simulations. Figure 4 shows the L^2 -norm of $C_{\Psi_0, \Psi_1, \Psi_2}$ for the equal-mass system. We can see they converge with resolution. In contrast, waveforms extracted using CCE from standard Cauchy evolutions without matching (dotted lines) show much poorer convergence.

Finally, we evaluate the numerical efficiency of our CCM code. Since the characteristic system is more efficient in handling the wave zone, CCM is expected to improve computational efficiency by reducing the size of the Cauchy domain [40]. Table I summarizes the CPU hours used by the CCM simulations and their corresponding reference systems. Even without full optimization, all three CCM simulations are already 1.8 – 3 times more efficient.

B. Quasi-head-on collisions

Our second class of simulations includes four quasi-head-on collisions of equal-mass nonspinning BHs. As summarized in Table I, we systematically increase the initial angular velocity Ω_{orb} (the transverse velocity relative to the line connecting the two BHs), while fixing the initial radial velocity at 0. In the special scenario where $\Omega_{\text{orb}} = 0$, the system reduces to the purely head-on scenario studied in Sec. III A.

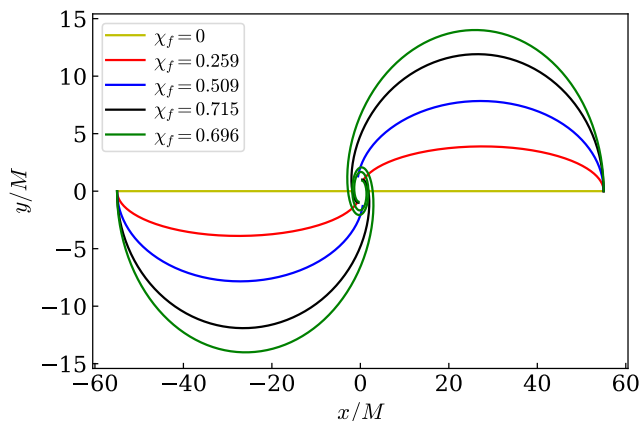


Figure 5. Trajectories of the BHs in the $x - y$ plane for the (quasi-)head-on systems listed in Table I. The initial angular velocity is along the z -axis. Each system is labeled by the dimensionless spin (χ_f) of the remnant Kerr BH.

Figure 5 shows the trajectories of the BHs in the $x - y$ plane (the initial angular velocity is along the z -axis). As Ω_{orb} increases, the BHs undergo a partial orbital motion before merging. Here we ensure that Ω_{orb} remains small to prevent an eccentric orbit. The remnants of

these collisions are Kerr BHs, whose dimensionless spins (χ_f) are listed in Table I. Notably, χ_f does not increase monotonically with Ω_{orb} , as a larger fraction of angular momentum may be radiated away in GWs during the inspiral phase. Below, for convenience, we use χ_f to label these quasi-head-on systems.

Figure 6 compares $\Psi_4^{\ell=2, m=0}$ extracted from CCM (in black), CCE (in blue), and reference systems (in red). Once again, we observe noticeable improvements in the CCM waveforms compared to CCE. In particular, the cases shown in Figs. 6c and 6d have relatively large initial angular velocities, leading to pre-ringdown GW emission. Their reference results display numerical wiggles in the late-time tail, whereas the CCM waveforms (using the same numerical resolution) remain accurate. Notably, as summarized in Table I, the CCM simulations require 2 – 3 times fewer CPU hours than the reference runs. These comparisons demonstrate that our CCM algorithm improves both waveform accuracy and computational efficiency.

Finally, we monitor the constraint violations throughout the simulations. As a representative case, we select the system in Fig. 6d, which has the largest initial angular velocity and the most complex pre-merger dynamics. Figure 7 provides the L^2 -norm of its GH constraint energy and $C_{\Psi_0, \Psi_1, \Psi_2}$. The results are consistent with our findings in Sec. III A and Paper I: (1) The CCM constraints converge with resolution. (2) CCM improves the characteristic constraints while keeping the GH constraint energy comparable to the systems without matching.

C. Eccentric binary

Our CCM simulations in Secs. III A and III B are relatively short and have simple pre-merger dynamics. To probe the long-term behavior of the algorithm, we now consider an eccentric binary system with randomly chosen initial angular and radial velocities, as listed in Table I. The initial separation is set to $90M$.

Figure 8 shows the trajectories of the two component BHs. The orbit begins with a large eccentricity (> 0.8) and exhibits strong perihelion precession. Over the 22.4 orbital cycles (~ 44.8 GW cycles) before the merger, the orbit gradually circularizes due to GW emission. The merger time is $14781M$, roughly 10 times longer than those studied in Secs. III A and III B. Given the long duration of the simulation, evolving the corresponding reference system becomes computationally impractical.

As in previous cases, no instabilities are observed in the CCM evolution. Figure 9 shows the full inspiral-merger-ringdown waveform $\Psi_4^{\ell=2, m=0}$ computed using CCM (in black) and CCE (in blue). During the inspiral stage, sharp bursts of GW radiation are emitted near each perihelion passage. Following the ringdown, a late-time tail is clearly visible, but this component is obscured by an error floor in the absence of CCM.

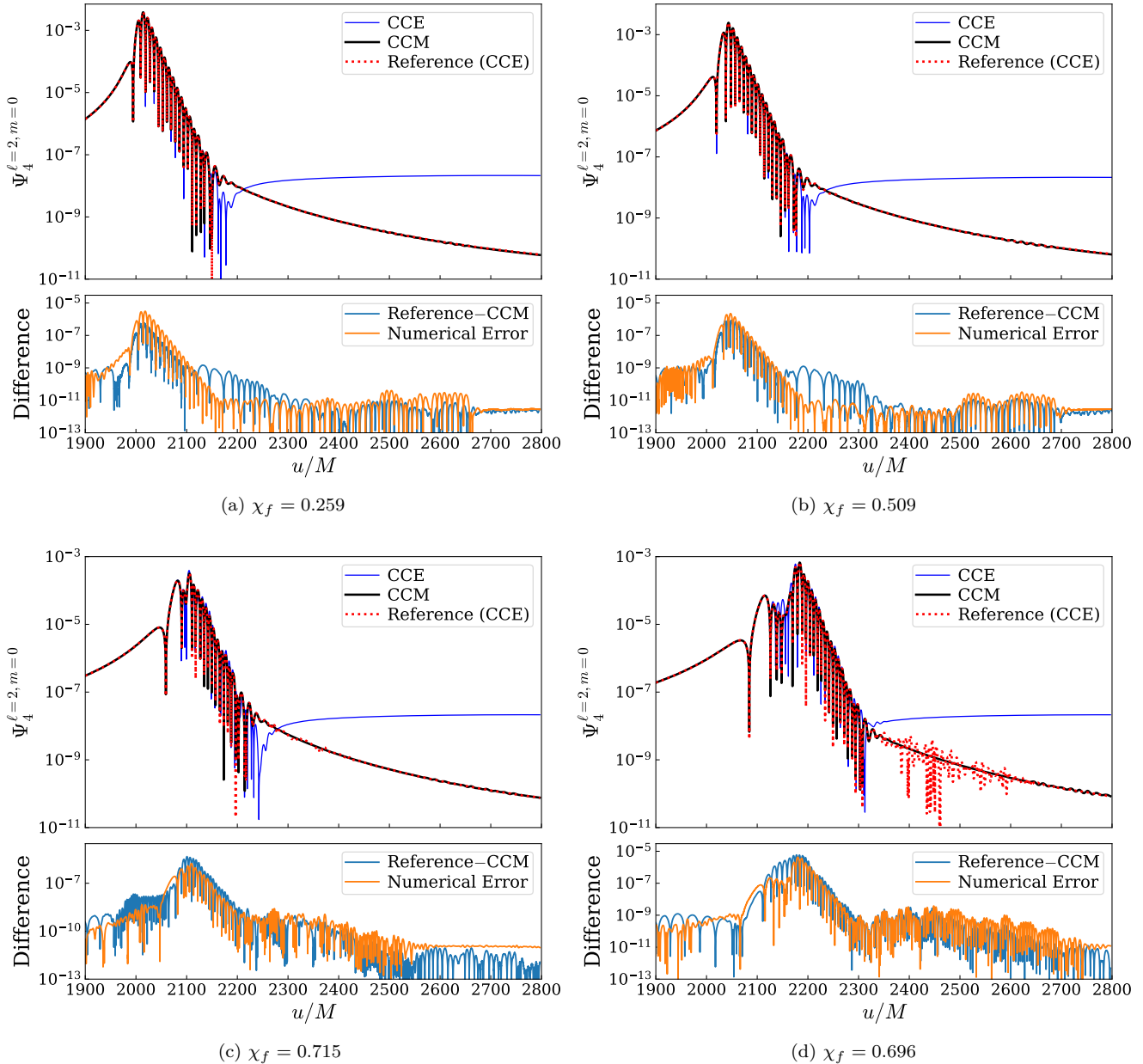


Figure 6. Similar to Fig. 1, comparison of $\Psi_4^{\ell=2, m=0}$ extracted from CCE, CCM, and reference systems for the quasi-head-on collisions listed in Table I. The initial angular velocity Ω_{orb} increases from (a) to (d), but the dimensionless spin of the remnant Kerr BHs (χ_f) does not increase monotonically — more angular momentum is radiated away via GWs in Fig. 6d than in Fig. 6c. Additionally, high- Ω_{orb} systems (Figs. 6c and 6d) exhibit pre-ringdown emission.

D. Quasi-circular binary

Our final case is a merger of two equal-mass, nonspinning BHs on a quasi-circular orbit. The properties of this system are summarized in Table I. The orbital eccentricity is iteratively reduced to below $\sim 4 \times 10^{-4}$ [125–127]. Figure 10 compares $\Psi_4^{\ell=m=2}$ extracted with and without CCM. In this case, the improvement from CCM is negligible, and there is no hint of late-time tails.

IV. TAIL ANALYSIS WITH RATIONAL FILTERS

CCM has opened a systematic path for studying late-time tails in BBH systems. Building on the results in Sec. III, we now present a phenomenological analysis of the tail behavior in the (quasi-)head-on configurations listed in Table I.

One challenge in tail extraction is the impact of QNMs, which can mask the tail signal, especially at early times. A common workaround is to delay the analysis window

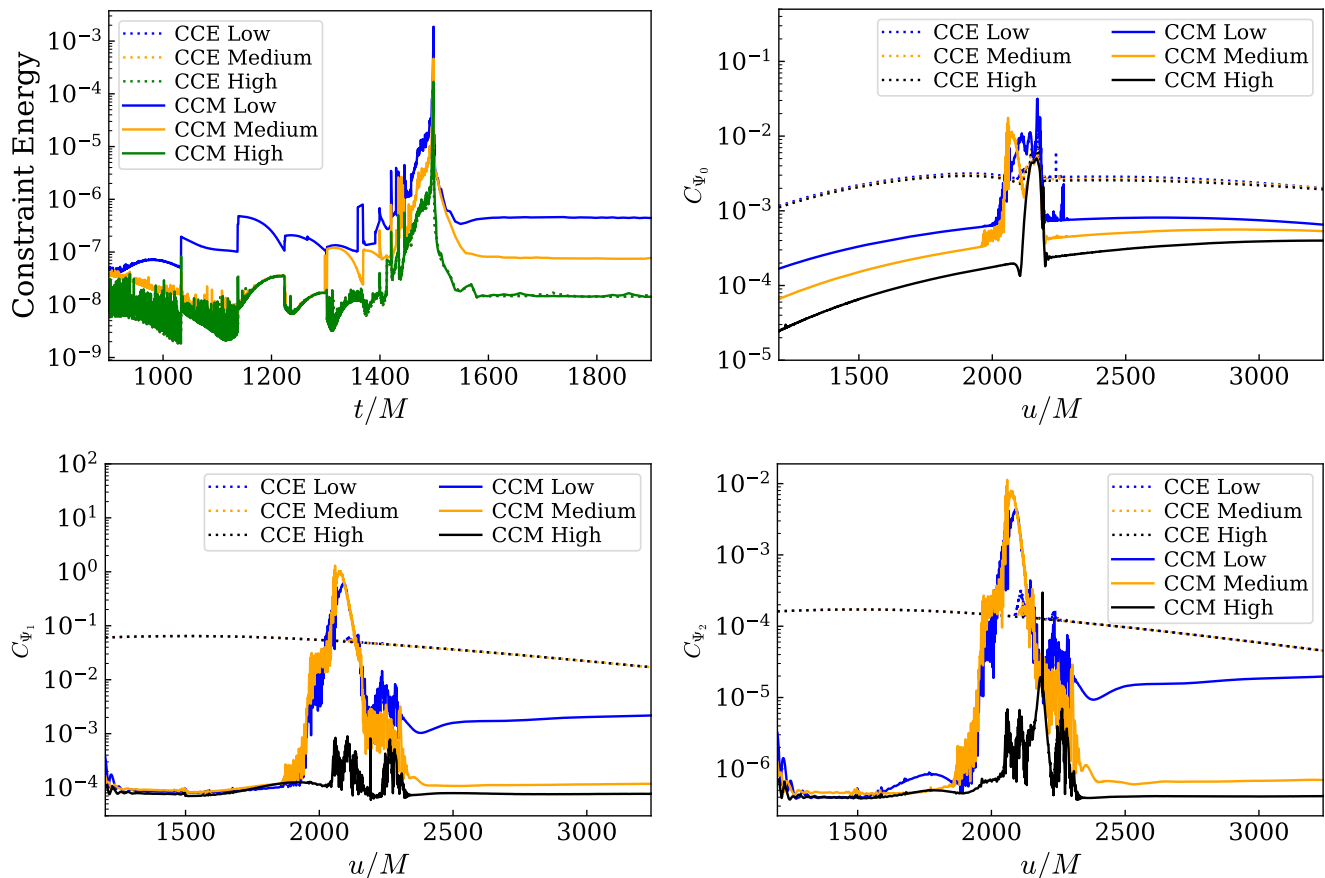


Figure 7. Similar to Figs. 3 and 4, L^2 -norm of the Cauchy GH constraint energy (top left) and C_{Ψ_0} , C_{Ψ_1} , C_{Ψ_2} for the system in Fig. 6d, using CCM (solid curves) and CCE (dotted curves).

until the QNMs have sufficiently decayed. However, this approach often results in unnecessary signal loss, particularly in NR waveforms. Moreover, the tail component may already be present beneath the QNM ringing at earlier times. The workaround risks overlooking the early-time contribution.

To overcome this, we adopt QNM rational filters [128–130] and the PYTHON package `qnm_filter` [131]. The filters enable mode removal given only their complex frequencies, without requiring knowledge of the corresponding mode amplitudes. This feature is particularly important, as accurate amplitude fitting demands a detailed model of the early-time tail — precisely the component we aim to isolate. The filters effectively break this circular dependency and provide a cleaner separation of tail and QNM content.

We first apply the Fourier-analysis method from Sec. III B of [132] to identify QNMs in $\Psi_4^{\ell=2,m=0}$. The extracted modes are listed in Table II. In particular, we find a few quadratic QNMs. We follow the labeling conventions of [133]. A linear QNM is labeled by four indices (ℓ, m, n, p) , where (ℓ, m) denote the angular harmonic indices; n is the overtone number; and $p = \text{sgn}(\text{Re}\omega)$ indicates the sign of the real part of the mode frequency.

Two modes with the same (ℓ, m, n) but opposite p are the mirror of each other. A quadratic mode is labeled by $(\ell_1, m_1, n_1, p_1; \ell_2, m_2, n_2, p_2)$, with its complex frequency given by the sum of the constituent linear mode frequencies.

After filtering out the QNMs from the ringdown regime, the resulting filtered waveforms are shown as red curves in the upper panels of Figs. 11 and 12. The time axis has been adjusted such that the peak of the original $\Psi_4^{\ell=2,m=0}$ occurs at $u = 0$. As noted in Sec. II B and Fig. 3 of [128], these filters introduce a backward time shift in power-law tails, with an analytical expression provided in Eq. (16) therein. We have verified that this formula accurately describes our case. Therefore, we apply this formula to adjust for the time shift in the following analysis.

The filters extend the duration of the nonoscillatory regime, while ensuring that the late-time portion remains accurately aligned with the raw $\Psi_4^{\ell=2,m=0}$ (green curves in the upper panels of Figs. 11 and 12). Using the fitting windows listed in Table II, we find that each filtered waveform can be well described by a single power law:

$$A(u + u_0)^p. \quad (5)$$

To improve fitting performance, we borrow the spirit of

Table II. Tail analysis for (quasi-)head-on binaries listed in Table I. Each case is labeled by the dimensionless spin χ_f of the remnant Kerr BH. The Weyl scalar Ψ_4 is filtered using rational filters constructed from the corresponding QNM contents, following the labeling conventions of Ref. [133]. The filtered Ψ_4 is fit to a single power law model in Eq. (5), within a specified time window.

| Systems | χ_f | Fitting Window | A | u_0 | p | QNM contents |
|---------------|----------|----------------|------------|-------|-------|--|
| Head-on | ~ 0 | $[50M, 400M]$ | 22.7η | 19.1 | -3.79 | $(2, 0, 0, \pm), (2, 0, 1, \pm)$ $(2, 0, 0, \pm; 2, 0, 0, \pm)$ |
| | 0.259 | $[50M, 400M]$ | 4.53 | 18.5 | -3.75 | $(2, 0, 0, \pm), (2, 0, 1, \pm), (2, 2, 0, \pm), (3, 2, 0, \pm)$ $(2, 0, 0, \pm; 2, 0, 0, \pm), (2, 2, 0, \pm; 2, 2, 0, \pm)$ |
| Quasi-Head-on | 0.509 | $[50M, 400M]$ | 3.74 | 19.4 | -3.73 | $(2, 0, 0, \pm), (2, 0, 1, \pm), (2, 2, 0, \pm), (3, 2, 0, \pm)$ $(3, 0, 0, \pm), (2, 0, 0, \pm; 2, 0, 0, \pm)$ |
| | 0.715 | $[80M, 400M]$ | 3.28 | 31.0 | -3.71 | $(2, 0, 0, \pm), (2, 0, 1, \pm), (2, 2, 0, \pm), (3, 2, 0, \pm)$ $(3, 0, 0, \pm), (2, 0, 0, \pm; 2, 0, 0, \pm)$ |
| | 0.696 | $[80M, 400M]$ | 0.86 | 55.6 | -3.51 | $(2, 0, 0, \pm), (2, 0, 1, \pm), (2, 2, 0, \pm), (3, 2, 0, \pm)$ $(3, 0, 0, \pm), (2, 0, 0, \pm; 2, 0, 0, \pm)$ |

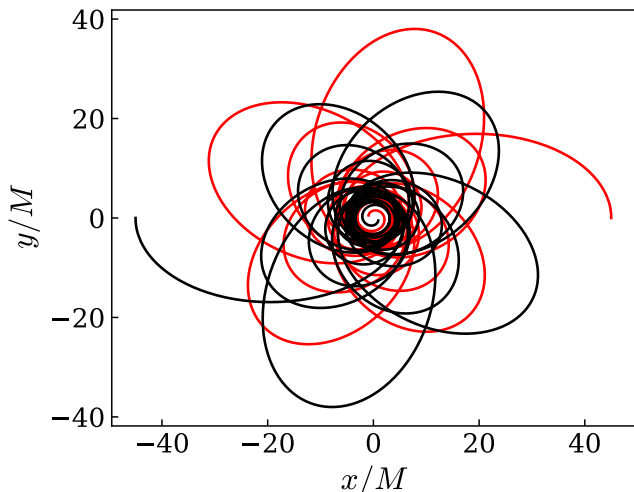


Figure 8. Trajectories of the BHs in the $x - y$ plane for the eccentric system listed in Table I. The initial angular velocity is along the z -axis.

variable projection [134, 135] by separating linear parameters from nonlinear ones. This step reduces a multidimensional fitting problem to a 1D problem. We have checked that the fits are highly stable against the initial guess. For more details, see the discussion around Eq. (73) in [74]. The residuals of the fits are provided in the lower panels of Figs. 11 and 12, where they are compared to an estimate of numerical error (the difference between two adjacent CCM resolutions). The residuals and error estimates are comparable, confirming that the single power-law model reasonably describes the filtered waveforms in the selected time windows.

The extracted fitting parameters A , u_0 , and p are summarized in Table II. For the head-on cases, we have factored out the symmetric mass ratio η [Eq. (3)], motivated by the scaling $\Psi_4 \propto \eta$ observed in Fig. 2. The results

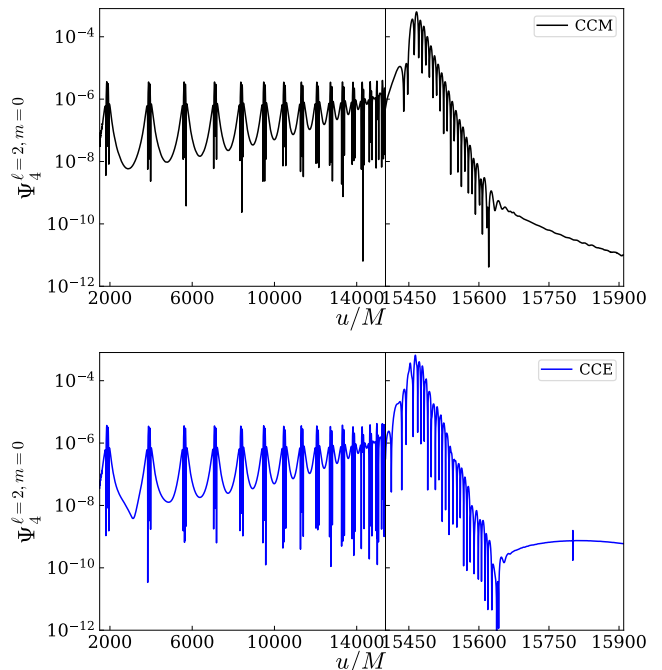


Figure 9. Inspiral-merger-ringdown $\Psi_4^{\ell=2, m=0}$ extracted using CCM (top panel) and CCE (bottom panel) from the eccentric system listed in Table I.

show that the tail amplitude A systematically decreases as the initial orbital angular velocity (Ω_{orb} in Table I) increases — or equivalently, as the orbital angle before merger grows. In contrast, there is no strong correlation between A and the spin of the remnant Kerr BH (χ_f). Similarly, the time parameter u_0 correlates more strongly with Ω_{orb} than with χ_f .

The power-law exponent p lies in the range -3.51 to -3.79 , which differs from the Price law u^{-6} for $\Psi_4^{\ell=2, m=0}$ [94, 95]. We propose two possible origins of the tail:

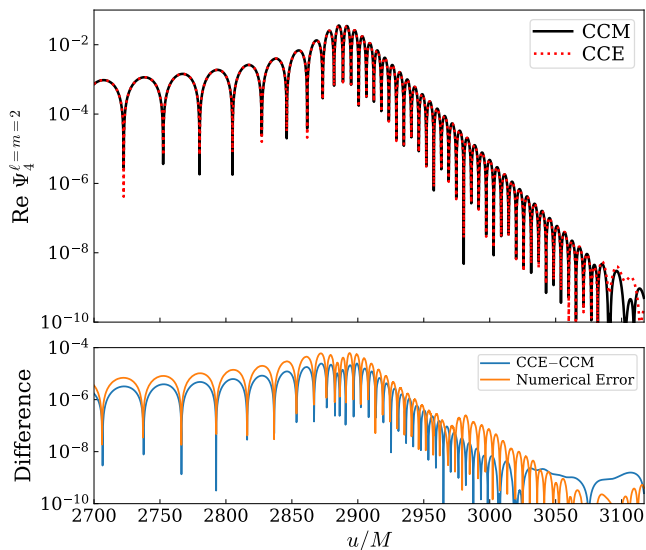


Figure 10. Top panel: $\Psi_4^{\ell=m=2}$ from a quasi-circular collision, simulated using CCM (black) and CCE (red). Bottom panel: The difference between the two results (blue), compared to the numerical error (orange).

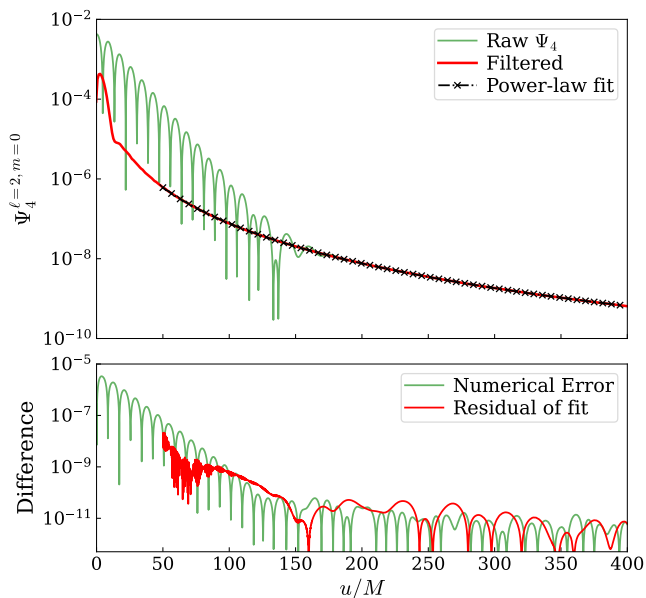


Figure 11. Top panel: The raw (green) and filtered (red) $\Psi_4^{\ell=2, m=0}$ simulated using CCM for the head-on collision of two equal-mass, nonspinning BHs. The power-law fit in Eq. (5) and Table II is shown in black (marked with crosses). Bottom panel: The residual of the power-law fit (red), compared to the numerical error (green) by taking the difference between two adjacent CCM resolutions.

- Intermediate regime of a linear tail. As shown in Fig. 4 of [136], the tail component requires $u > 10^4$ to fully converge to the Price law. At $u \gtrsim 100$, the exponent ranges from -3.5 to -4.2 (our exponent

for Ψ_4 differs from the strain exponent in [136] by 2). The extracted exponents fall within this range and are consistent with this intermediate linear regime.

- QNM-driven “tail”. As discussed in [137, 138], an outgoing QNM generates a quadratic source that falls polynomially with distance. At second order, it yields a power-law decay in GWs, expected to follow u^{-4} in Ψ_4 [Eq. (66) in [137]³]. Since this decays slower than the Price law, the nonlinearity likely dominates at late times. The presence of quadratic QNMs supports this possibility.

Both channels produce similar power laws in our window⁴. Distinguishing them requires further study. First, as in [122], one needs to perform a systematic comparison between linear-theory predictions and CCM results across a range of BBH configurations. Second, the QNM-driven channel might establish a determined link between the tail and the quadratic QNM, similar to the quadratic-to-linear ratio in [133, 141]. Using the source term in the second-order Teukolsky equation [see Eq. (54) in [141]], one can make theoretical predictions for the parameters in Eq. (5) and compare them against our extracted values. We leave these discussions for future work.

V. CONCLUSION

We have addressed that CCM, a framework originally proposed in the 1990s [40, 77], is not only feasible but also enables stable, convergent, and high-accuracy simulations of BBH mergers on an effectively infinite computational domain. By evolving nine BBH systems with the algorithm detailed in Paper I, we showed that their waveforms are in excellent agreement with those from reference simulations with distant outer boundaries, which avoid contamination from inaccurate boundary conditions. In contrast, CCE results exhibited systematic errors.

Thanks to its unprecedented waveform accuracy, CCM makes it possible to systematically study late-time tails in the fully nonlinear regime. Using rational filters [128–130], we isolated tail components in (quasi-)head-on binary systems from QNMs. Within selected fitting windows, the filtered waveforms were well described by power laws. The tail amplitudes decrease as the initial orbital angular momentum increases, while the power-law exponents range from -3.51 to -3.79 . We proposed two possible origins for the phenomenon: either the intermediate regime of the linear tail or the QNM-driven nonlinear tail [137, 138]. To distinguish between these two channels, further work

³ The exact exponent may remain uncertain, as the authors found discrepancies between some numerical simulations and analytical predictions.

⁴ QNMs also produce power-law decays via other channels [139, 140].

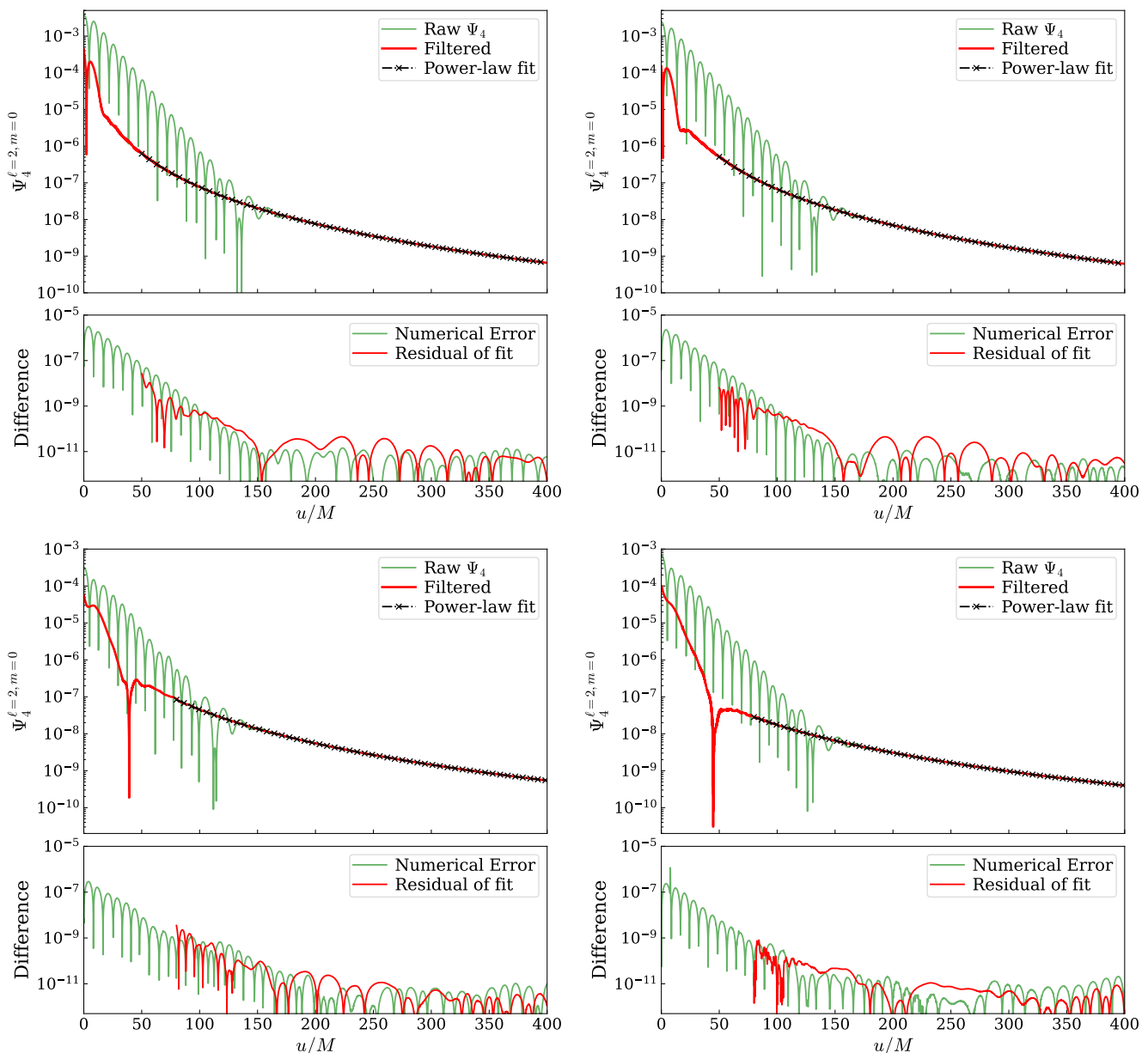


Figure 12. Similar to Fig. 11, tail analysis for the quasi-head-on binary systems listed in Table I.

is needed: (i) systematic comparisons between linear calculations [136, 142, 143] and CCM results; and (ii) precise theoretical predictions for the nonlinear tail from second-order black hole perturbation theory [133, 141]. If confirmed as nonlinear, this would be an example where nonlinearity prevails over linearity at late times.

In this work, we have focused on the tail and ring-down regimes of the Weyl scalar Ψ_4 to provide preliminary evidence that CCM effectively removes boundary-induced systematics. A more comprehensive investigation of the GW strain across the full inspiral–merger–ringdown regime is still needed. In particular, it would be interesting to explore whether CCM can resolve tail effects during the inspiral phase through comparisons with post-

Newtonian predictions.

Although we have demonstrated that our CCM simulations are stable, convergent, and highly accurate — at least for the nine BBH systems — a common concern about CCM in the literature is that it might be only weakly hyperbolic [40, 88–92], which appears to be in tension with our results. Gundlach [92] has recently provided a tentative solution: by introducing an alternative energy norm, the linearized characteristic initial-boundary value problem about Schwarzschild is shown to be well-posed, and it is conjectured that this result generalizes to arbitrary backgrounds. Given our numerical progress here and in Paper I — especially its implications for tail and high-accuracy waveform modeling — it seems timely to

address the tension, particularly in the context of the specific CCM formulation we employ.

Finally, as discussed in Paper I and summarized in Sec. II, the detailed implementation of CCM depends on the underlying Cauchy formalism. For instance, unlike the Cauchy-perturbative matching strategies in [85–87] or [144], the GH formalism [99, 100] offers a neat decomposition of the forty incoming characteristic fields into three subsets, allowing us to focus only on the “physical” subset with just two degrees of freedom. It would be interesting to investigate whether matching this minimal set of dynamical variables is essential to ensure CCM stability, and how CCM can be adapted to other Cauchy formulations.

ACKNOWLEDGMENTS

S. M. would like to thank Luis Lehner, Conner Daley, and Eric Poisson for useful discussions. Research at Perimeter Institute is supported in part by the Government of Canada through the Department of Innovation, Science and Economic Development and by the Province of Ontario through the Ministry of Colleges and Universities. This material is based upon work supported by the National Science Foundation under Grants No. PHY-2407742, No. PHY-2207342, and No. OAC-2209655 at Cornell. Any opinions, findings, and conclusions or recommendations expressed in this material are those of the author(s) and do not necessarily reflect the views of the National Science Foundation. This work was supported by the Sherman Fairchild Foundation at Cornell. This work was supported in part by the Sherman Fairchild Foundation and by NSF Grants No. PHY-2309211, No. PHY-2309231, and No. OAC-2209656 at Caltech. The computations presented here were conducted in the Resnick High Performance Computing Center, a facility supported by Resnick Sustainability Institute at the California Institute of Technology.

Appendix A: The characteristic initial data

Currently, SpECTRE supports various options for constructing characteristic initial data empirically. Although, in principle, the initial data should be *uniquely* determined from an *ab initio* approach, the default method known as `ConformalFactor` [145] in SpECTRE has proven to be a suitable choice [76]. In particular, it can help reduce initial junk radiation in the memory modes of BBH systems (see discussions below). Providing a comprehensive discussion on how characteristic initial data affects GW waveforms [146] and developing an *ab initio* initial-data solver is beyond the scope of this paper. Here we give a brief summary of the `ConformalFactor` method, as it was not fully explained in [47].

The SpECTRE characteristic system evolves two scalars and a vector, including

- Bondi J : This complex scalar is a volume variable that depends on both angular and radial coordinates. Its evolution is governed by a hierarchical system, see e.g., Eqs. (14)–(18) in [45].
- Cauchy angular coordinates $x^A = (\theta, \phi)$: These coordinates form a real vector defined on an extraction worldtube, usually chosen to be a sphere. Cauchy’s angular coordinates do not align with those of the characteristic system — they evolve over time with respect to the characteristic coordinates. The evolution equation can be found in Eq. (4.53) of [93]. This time-dependent mapping between the two coordinate systems is crucial for variable interpolation on the worldtube.
- Bondi time \hat{u} : The SpECTRE characteristic system adopts the so-called partially flat Bondi-like coordinates, see Table I in [46] and Fig. 1 in [93], whose time coordinate differs from the true Bondi time. The two time coordinates are related via $\hat{u} = \int e^{2\beta} du + \hat{u}^{(R)}$, see Eq. (35) in [46] for more details. Here β is the variable that appears in the Bondi metric, see e.g. Eq. (1) in [46]. The mapping can be interpreted as a BMS transformation: the term involving $e^{2\beta}$ yields time dilation via the conformal factor ω in Eq. (2.12a) of [147], while $\hat{u}^{(R)}$ contributes to a supertranslation. Waveform quantities are asymptotically transformed into the true Bondi frame only at the output stage. The BMS transformations for these waveform quantities can be found in Eq. (94) of [46], consistent with Eq. (17) of [121].

Initial data are needed for all of these evolved variables.

For the Bondi time \hat{u} , its initial data sets the angular-dependent integration constant for $\hat{u} = \int e^{2\beta} du$, which reflects the supertranslation freedom of the first characteristic slice. Currently, the constant is hard-coded to zero in SpECTRE.

The initialization of J is based on the cubic ansatz, see Eq. (16) of [47]

$$J = \frac{A}{r} + \frac{B}{r^3}. \quad (\text{A1})$$

The coefficients A and B are determined by the worldtube data for J and $\partial_r J$ taken from a Cauchy evolution. Here the term $1/r^2$ is omitted to avoid logarithmic terms, see Sec. V B of [46].

The initial data for the Cauchy angular coordinates x^A deserves more attention. Denoting the characteristic angular coordinates as $\hat{x}^{\hat{A}}$, the mapping between them is controlled by the Jacobian $\partial_{\hat{A}} x^A$. In SpECTRE, the Jacobian is represented by two complex scalars $\hat{a} = \hat{q}^{\hat{A}} \partial_{\hat{A}} x^A q_A$ and $\hat{b} = \hat{\bar{q}}^{\hat{A}} \partial_{\hat{A}} x^A q_A$ [see Eq. (4.13) of [93]]

$$\partial_{\hat{A}} x^A = \frac{1}{4} \left(\hat{q}_{\hat{A}}, \hat{\bar{q}}_{\hat{A}} \right) \begin{pmatrix} \hat{\bar{a}} & \hat{\bar{b}} \\ \hat{b} & \hat{a} \end{pmatrix} \begin{pmatrix} q^A \\ \bar{q}^A \end{pmatrix}, \quad (\text{A2})$$

where the dyad q^A is given by $(-1, -i \csc \theta)$. Treating the Jacobian as a 2×2 matrix, its determinant $\hat{\omega}$ can be computed via

$$\hat{\omega}^2 = \frac{1}{2} \epsilon_{AB} \epsilon^{\hat{A}\hat{B}} \partial_{\hat{A}} x^A \partial_{\hat{B}} x^B = \frac{1}{4} (\hat{b}\hat{b} - \hat{a}\hat{a}), \quad (\text{A3})$$

where $\epsilon_{AB} = \frac{i}{2} q_A \wedge \bar{q}_B$ is the volume form compatible with the unit sphere metric. To obtain Eq. (A3), we have used $q^A \epsilon_{AB} = -i q_B$.

Similar to BMS symmetries, where a conformal isometry of the 2-sphere leads to time dilation, see Eq. (2.12a) of [147], the angular diffeomorphism in the present case also leads to the transformation of the Bondi β [Eq. (33a) of [46]]

$$e^{2\hat{\beta}} = e^{2\beta} / \hat{\omega}, \quad (\text{A4})$$

where the value of β on a worldtube comes from a Cauchy evolution, and the transformed $\hat{\beta}$ is defined in the partially flat Bondi-like coordinates, used for future hypersurface integration. **SpECTRE** now sets the initial value of $\hat{\beta}$ to zero, which yields an algebraic equation for the Jacobian:

$$e^{2\beta} = \hat{\omega} = \frac{1}{2} \sqrt{\hat{b}\hat{b} - \hat{a}\hat{a}}. \quad (\text{A5})$$

where we have used Eq. (A3). Since the determinant $\hat{\omega}$ plays a similar role as the conformal factor in BMS, this method is thus termed **ConformalFactor**. In the code, Eq. (A5) is iteratively inverted to solve for the scalars \hat{a} and \hat{b} , thereby constructing $x^A(\hat{x}^{\hat{A}})$. Roughly speaking, Eq. (A5) sets the initial ‘‘lapse’’ at the worldtube to unity, aligning the clock rate with that of inertial observers at future null infinity.

The initial condition for $x^A(\hat{x}^{\hat{A}})$ is crucial in reducing the junk radiation in memory modes, see the red curve in Fig. 10 of [75]. There, a less motivated initial condition $\hat{x}^{\hat{A}} = \delta_{\hat{A}}^A x^A$ was used⁵.

REFERENCES

- [1] B. P. Abbott *et al.* (LIGO Scientific, Virgo), Binary Black Hole Mergers in the first Advanced LIGO Observing Run, *Phys. Rev. X* **6**, 041015 (2016), [erratum: *Phys. Rev. X* **8**, no.3, 039903(2018)], [arXiv:1606.04856 \[gr-qc\]](#).
- [2] B. P. Abbott *et al.* (LIGO Scientific, Virgo), GWTC-1: A Gravitational-Wave Transient Catalog of Compact Binary Mergers Observed by LIGO and Virgo during the First and Second Observing Runs, *Phys. Rev. X* **9**, 031040 (2019), [arXiv:1811.12907 \[astro-ph.HE\]](#).
- [3] R. Abbott *et al.* (LIGO Scientific, Virgo), GWTC-2: Compact Binary Coalescences Observed by LIGO and Virgo During the First Half of the Third Observing Run, *Phys. Rev. X* **11**, 021053 (2021), [arXiv:2010.14527 \[gr-qc\]](#).
- [4] R. Abbott *et al.* (LIGO Scientific, VIRGO, KAGRA), GWTC-3: Compact Binary Coalescences Observed by LIGO and Virgo During the Second Part of the Third Observing Run, (2021), [arXiv:2111.03606 \[gr-qc\]](#).
- [5] J. Aasi *et al.* (LIGO Scientific), Advanced LIGO, *Class. Quant. Grav.* **32**, 074001 (2015), [arXiv:1411.4547 \[gr-qc\]](#).
- [6] F. Acernese *et al.* (Virgo), Advanced Virgo: a second-generation interferometric gravitational wave detector, *Class. Quant. Grav.* **32**, 024001 (2015), [arXiv:1408.3978 \[gr-qc\]](#).
- [7] K. Somiya (KAGRA), Detector configuration of KAGRA: The Japanese cryogenic gravitational-wave detector, *Class. Quant. Grav.* **29**, 124007 (2012), [arXiv:1111.7185 \[gr-qc\]](#).
- [8] Y. Pan, A. Buonanno, L. T. Buchman, T. Chu, L. E. Kidder, H. P. Pfeiffer, and M. A. Scheel, Effective-one-body waveforms calibrated to numerical relativity simulations: coalescence of non-precessing, spinning, equal-mass black holes, *Phys. Rev. D* **81**, 084041 (2010), [arXiv:0912.3466 \[gr-qc\]](#).
- [9] A. Bohé *et al.*, Improved effective-one-body model of spinning, nonprecessing binary black holes for the era of gravitational-wave astrophysics with advanced detectors, *Phys. Rev. D* **95**, 044028 (2017), [arXiv:1611.03703 \[gr-qc\]](#).
- [10] L. Pompili *et al.*, Laying the foundation of the effective-one-body waveform models SEOBNRv5: Improved accuracy and efficiency for spinning nonprecessing binary black holes, *Phys. Rev. D* **108**, 124035 (2023), [arXiv:2303.18039 \[gr-qc\]](#).
- [11] A. Nagar *et al.*, Time-domain effective-one-body gravitational waveforms for coalescing compact binaries with nonprecessing spins, tides and self-spin effects, *Phys. Rev. D* **98**, 104052 (2018), [arXiv:1806.01772 \[gr-qc\]](#).
- [12] A. Nagar, G. Riemenschneider, G. Pratten, P. Rettengo, and F. Messina, Multipolar effective one body waveform model for spin-aligned black hole binaries, *Phys. Rev. D* **102**, 024077 (2020), [arXiv:2001.09082 \[gr-qc\]](#).
- [13] J. Blackman, S. E. Field, M. A. Scheel, C. R. Galley, C. D. Ott, M. Boyle, L. E. Kidder, H. P. Pfeiffer, and B. Szilágyi, Numerical relativity waveform surrogate model for generically precessing binary black hole mergers, *Phys. Rev. D* **96**, 024058 (2017), [arXiv:1705.07089 \[gr-qc\]](#).
- [14] V. Varma, S. E. Field, M. A. Scheel, J. Blackman, L. E. Kidder, and H. P. Pfeiffer, Surrogate model of hybridized numerical relativity binary black hole waveforms, *Phys. Rev. D* **99**, 064045 (2019), [arXiv:1812.07865 \[gr-qc\]](#).
- [15] V. Varma, S. E. Field, M. A. Scheel, J. Blackman, D. Gerosa, L. C. Stein, L. E. Kidder, and H. P. Pfeiffer, Surrogate models for precessing binary black hole simulations with unequal masses, *Phys. Rev. Research* **1**, 033015 (2019), [arXiv:1905.09300 \[gr-qc\]](#).
- [16] J. Yoo *et al.*, Numerical relativity surrogate model with memory effects and post-Newtonian hybridization, *Phys. Rev. D* **108**, 064027 (2023), [arXiv:2306.03148 \[gr-qc\]](#).
- [17] R. Abbott *et al.* (LIGO Scientific, Virgo), Population Properties of Compact Objects from the Second LIGO-Virgo Gravitational-Wave Transient Catalog, *Astrophys. J. Lett.* **913**, L7 (2021), [arXiv:2010.14533 \[astro-ph.HE\]](#).
- [18] R. Abbott *et al.* (LIGO Scientific, Virgo), Tests of general relativity with binary black holes from the second LIGO-Virgo gravitational-wave transient catalog, *Phys. Rev. D* **103**, 122002 (2021), [arXiv:2010.14529 \[gr-qc\]](#).

⁵ The Bondi J was still constructed using Eq. (A1).

- [19] R. Abbott *et al.* (LIGO Scientific, Virgo), GW190521: A Binary Black Hole Merger with a Total Mass of $150 M_{\odot}$, *Phys. Rev. Lett.* **125**, 101102 (2020), arXiv:2009.01075 [gr-qc].
- [20] R. Abbott *et al.* (LIGO Scientific, Virgo), GW190412: Observation of a Binary-Black-Hole Coalescence with Asymmetric Masses, *Phys. Rev. D* **102**, 043015 (2020), arXiv:2004.08342 [astro-ph.HE].
- [21] R. Abbott *et al.* (LIGO Scientific, Virgo), Properties and Astrophysical Implications of the $150 M_{\odot}$ Binary Black Hole Merger GW190521, *Astrophys. J.* **900**, L13 (2020), arXiv:2009.01190 [astro-ph.HE].
- [22] R. Abbott *et al.* (LIGO Scientific, VIRGO, KAGRA), Search for intermediate-mass black hole binaries in the third observing run of Advanced LIGO and Advanced Virgo, *Astron. Astrophys.* **659**, A84 (2022), arXiv:2105.15120 [astro-ph.HE].
- [23] R. Abbott *et al.* (LIGO Scientific, VIRGO), Search for Lensing Signatures in the Gravitational-Wave Observations from the First Half of LIGO–Virgo’s Third Observing Run, *Astrophys. J.* **923**, 14 (2021), arXiv:2105.06384 [gr-qc].
- [24] M. Pürrer and C.-J. Haster, Gravitational waveform accuracy requirements for future ground-based detectors, *Phys. Rev. Res.* **2**, 023151 (2020), arXiv:1912.10055 [gr-qc].
- [25] T. W. Baumgarte and S. L. Shapiro, *Numerical Relativity: Solving Einstein’s Equations on the Computer* (Cambridge University Press, 2010).
- [26] E. W. Allen, E. Buckmiller, L. M. Burko, and R. H. Price, Radiation tails and boundary conditions for black hole evolutions, *Phys. Rev. D* **70**, 044038 (2004), arXiv:gr-qc/0401092.
- [27] M. Dafermos and I. Rodnianski, A Note on boundary value problems for black hole evolutions, (2004), arXiv:gr-qc/0403034.
- [28] A. Zenginoglu, Hyperboloidal evolution with the Einstein equations, *Class. Quant. Grav.* **25**, 195025 (2008), arXiv:0808.0810 [gr-qc].
- [29] O. Rinne and V. Moncrief, Hyperboloidal Einstein-matter evolution and tails for scalar and Yang-Mills fields, *Class. Quant. Grav.* **30**, 095009 (2013), arXiv:1301.6174 [gr-qc].
- [30] A. Vañó Viñuales, S. Husa, and D. Hilditch, Spherical symmetry as a test case for unconstrained hyperboloidal evolution, *Class. Quant. Grav.* **32**, 175010 (2015), arXiv:1412.3827 [gr-qc].
- [31] A. Vañó Viñuales and S. Husa, Unconstrained hyperboloidal evolution of black holes in spherical symmetry with GBSSN and Z4c, *J. Phys. Conf. Ser.* **600**, 012061 (2015), arXiv:1412.4801 [gr-qc].
- [32] M. D. Morales and O. Sarbach, Evolution of scalar fields surrounding black holes on compactified constant mean curvature hypersurfaces, *Phys. Rev. D* **95**, 044001 (2017), arXiv:1609.05756 [gr-qc].
- [33] A. Vañó Viñuales and T. Valente, Height-function-based 4D reference metrics for hyperboloidal evolution, *Gen. Rel. Grav.* **56**, 135 (2024), arXiv:2408.08952 [gr-qc].
- [34] C. Peterson, S. Gautam, A. Vañó Viñuales, and D. Hilditch, Spherical Evolution of the Generalized Harmonic Gauge Formulation of General Relativity on Compactified Hyperboloidal Slices, (2024), arXiv:2409.02994 [gr-qc].
- [35] H. Friedrich, Gravitational fields near space-like and null infinity, *Journal of Geometry and Physics* **24**, 83 (1998).
- [36] J. Frauendiener and C. Stevens, The non-linear perturbation of a black hole by gravitational waves. II. Quasi-normal modes and the compactification problem, *Class. Quant. Grav.* **40**, 125006 (2023), arXiv:2211.13276 [gr-qc].
- [37] J. Frauendiener, A. Goodenbour, and C. Stevens, The non-linear perturbation of a black hole by gravitational waves. III. Newman–Penrose constants, *Class. Quant. Grav.* **41**, 065005 (2024), arXiv:2301.05268 [gr-qc].
- [38] J. Frauendiener and C. Stevens, The non-linear perturbation of a black hole by gravitational waves. I. The Bondi–Sachs mass loss, *Class. Quant. Grav.* **38**, 194002 (2021), arXiv:2105.09515 [gr-qc].
- [39] J. Frauendiener, C. Stevens, and S. Thwala, Fully non-linear gravitational wave simulations from past to future null-infinity, (2025), arXiv:2504.02188 [gr-qc].
- [40] J. Winicour, Characteristic evolution and matching, *Living Reviews in Relativity* **15**, 1 (2012).
- [41] N. T. Bishop, Numerical relativity: combining the cauchy and characteristic initial value problems, *Classical and Quantum Gravity* **10**, 333 (1993).
- [42] N. T. Bishop, R. Gomez, L. Lehner, and J. Winicour, Cauchy-characteristic extraction in numerical relativity, *Phys. Rev. D* **54**, 6153 (1996), arXiv:gr-qc/9705033 [gr-qc].
- [43] N. T. Bishop, R. Gomez, L. Lehner, M. Maharaj, and J. Winicour, High powered gravitational news, *Phys. Rev. D* **56**, 6298 (1997), arXiv:gr-qc/9708065.
- [44] N. T. Bishop, R. Gomez, L. Lehner, B. Szilágyi, J. Winicour, and R. A. Isaacson, Cauchy characteristic matching, in *Black Holes, Gravitational Radiation and the Universe: Essays in Honor of C.V. Vishveshwara*, edited by B. R. Iyer and B. Bhawal (1998) pp. 383–408, arXiv:gr-qc/9801070.
- [45] K. Barkett, J. Moxon, M. A. Scheel, and B. Szilágyi, Spectral Cauchy-Characteristic Extraction of the Gravitational Wave News Function, *Phys. Rev. D* **102**, 024004 (2020), arXiv:1910.09677 [gr-qc].
- [46] J. Moxon, M. A. Scheel, and S. A. Teukolsky, Improved Cauchy-characteristic evolution system for high-precision numerical relativity waveforms, *Phys. Rev. D* **102**, 044052 (2020), arXiv:2007.01339 [gr-qc].
- [47] J. Moxon, M. A. Scheel, S. A. Teukolsky, N. Deppe, N. Fischer, F. Hébert, L. E. Kidder, and W. Throwe, SpECTRE Cauchy-characteristic evolution system for rapid, precise waveform extraction, *Phys. Rev. D* **107**, 064013 (2023), arXiv:2110.08635 [gr-qc].
- [48] R. Corkill and J. Stewart, Numerical relativity. ii. numerical methods for the characteristic initial value problem and the evolution of the vacuum field equations for spacetimes with two killing vectors, *Proceedings of the Royal Society of London. A. Mathematical and Physical Sciences* **386**, 373 (1983).
- [49] H. Friedrich and J. M. Stewart, Characteristic initial data and wavefront singularities in general relativity, *Proceedings of the Royal Society of London. A. Mathematical and Physical Sciences* **385**, 345 (1983).
- [50] J. M. Stewart, The characteristic initial value problem in general relativity, in *Astrophysical Radiation Hydrodynamics*, edited by K.-H. A. Winkler and M. L. Norman (Springer Netherlands, Dordrecht, 1986) pp. 531–568.
- [51] S. Frittelli and E. T. Newman, Singularities of wavefronts and lightcones in the context of GR via null foliations,

- Twistor Newslett. **43**, 14 (1997), [arXiv:gr-qc/0006077](#).
- [52] S. Bhagwat, M. Okounkova, S. W. Ballmer, D. A. Brown, M. Giesler, M. A. Scheel, and S. A. Teukolsky, On choosing the start time of binary black hole ringdowns, *Phys. Rev. D* **97**, 104065 (2018), [arXiv:1711.00926 \[gr-qc\]](#).
- [53] T. W. Baumgarte, B. Brügmann, D. Cors, C. Gundlach, D. Hilditch, A. Khirnov, T. Ledvinka, S. Renkhoff, and I. S. Fernández, Critical Phenomena in the Collapse of Gravitational Waves, *Phys. Rev. Lett.* **131**, 181401 (2023), [arXiv:2305.17171 \[gr-qc\]](#).
- [54] R. A. Isaacson, J. S. Welling, and J. Winicour, Null cone computation of gravitational radiation, *Journal of Mathematical Physics* **24**, 1824 (1983).
- [55] N. T. Bishop, Some aspects of the characteristic initial value problem in numerical relativity., in *Approaches to Numerical Relativity*, edited by R. D’Inverno (1992) pp. 20–33.
- [56] J. Winicour, Newtonian gravity on the null cone., *Journal of Mathematical Physics* **24**, 1193 (1983).
- [57] J. Winicour, Null infinity from a quasi-newtonian view, *Journal of Mathematical Physics* **25**, 2506 (1984).
- [58] N. T. Bishop, R. Gómez, P. R. Holvorcem, R. A. Matzner, P. Papadopoulos, and J. Winicour, Cauchy Characteristic Evolution and Waveforms, *Journal of Computational Physics* **136**, 140 (1997).
- [59] B. Szilagyí, *Cauchy characteristic matching in general relativity*, Other thesis (2000), [arXiv:gr-qc/0006091](#).
- [60] R. Gomez, P. Papadopoulos, and J. Winicour, Null cone evolution of axisymmetric vacuum space-times, *Journal of Mathematical Physics* **35**, 4184 (1994).
- [61] R. Gomez, Gravitational wave forms with controlled accuracy, *Phys. Rev. D* **64**, 024007 (2001), [arXiv:gr-qc/0103011](#).
- [62] N. T. Bishop and S. S. Deshingkar, New approach to calculating the news, *Phys. Rev. D* **68**, 024031 (2003), [arXiv:gr-qc/0303021](#).
- [63] C. Reisswig, N. T. Bishop, C. W. Lai, J. Thornburg, and B. Szilagyí, Numerical relativity with characteristic evolution, using six angular patches, *Class. Quant. Grav.* **24**, S327 (2007), [arXiv:gr-qc/0610019](#).
- [64] R. Gomez, W. Barreto, and S. Frittelli, A Framework for large-scale relativistic simulations in the characteristic approach, *Phys. Rev. D* **76**, 124029 (2007), [arXiv:0711.0564 \[gr-qc\]](#).
- [65] M. C. Babiuc, N. T. Bishop, B. Szilagyí, and J. Winicour, Strategies for the Characteristic Extraction of Gravitational Waveforms, *Phys. Rev. D* **79**, 084011 (2009), [arXiv:0808.0861 \[gr-qc\]](#).
- [66] C. Reisswig, N. T. Bishop, and D. Pollney, General relativistic null-cone evolutions with a high-order scheme, *Gen. Rel. Grav.* **45**, 1069 (2013), [arXiv:1208.3891 \[gr-qc\]](#).
- [67] C. Reisswig, N. T. Bishop, D. Pollney, and B. Szilagyí, Unambiguous determination of gravitational waveforms from binary black hole mergers, *Phys. Rev. Lett.* **103**, 221101 (2009), [arXiv:0907.2637 \[gr-qc\]](#).
- [68] C. Reisswig, N. T. Bishop, D. Pollney, and B. Szilagyí, Characteristic extraction in numerical relativity: binary black hole merger waveforms at null infinity, *Class. Quant. Grav.* **27**, 075014 (2010), [arXiv:0912.1285 \[gr-qc\]](#).
- [69] M. C. Babiuc, B. Szilagyí, J. Winicour, and Y. Zlochower, A Characteristic Extraction Tool for Gravitational Waveforms, *Phys. Rev. D* **84**, 044057 (2011), [arXiv:1011.4223 \[gr-qc\]](#).
- [70] M. C. Babiuc, J. Winicour, and Y. Zlochower, Binary Black Hole Waveform Extraction at Null Infinity, *Class. Quant. Grav.* **28**, 134006 (2011), [arXiv:1106.4841 \[gr-qc\]](#).
- [71] C. J. Handmer and B. Szilagyí, Spectral Characteristic Evolution: A New Algorithm for Gravitational Wave Propagation, *Class. Quant. Grav.* **32**, 025008 (2015), [arXiv:1406.7029 \[gr-qc\]](#).
- [72] C. J. Handmer, B. Szilagyí, and J. Winicour, Gauge Invariant Spectral Cauchy Characteristic Extraction, *Class. Quant. Grav.* **32**, 235018 (2015), [arXiv:1502.06987 \[gr-qc\]](#).
- [73] C. J. Handmer, B. Szilagyí, and J. Winicour, Spectral Cauchy Characteristic Extraction of strain, news and gravitational radiation flux, *Class. Quant. Grav.* **33**, 225007 (2016), [arXiv:1605.04332 \[gr-qc\]](#).
- [74] S. Ma, K. C. Nelli, J. Moxon, M. A. Scheel, N. Deppe, L. E. Kidder, W. Throwe, and N. L. Vu, Einstein–Klein–Gordon system via Cauchy-characteristic evolution: computation of memory and ringdown tail, *Class. Quant. Grav.* **42**, 055006 (2025), [arXiv:2409.06141 \[gr-qc\]](#).
- [75] K. Mitman, J. Moxon, M. A. Scheel, S. A. Teukolsky, M. Boyle, N. Deppe, L. E. Kidder, and W. Throwe, Computation of displacement and spin gravitational memory in numerical relativity, *Phys. Rev. D* **102**, 104007 (2020), [arXiv:2007.11562 \[gr-qc\]](#).
- [76] K. Mitman *et al.*, A review of gravitational memory and BMS frame fixing in numerical relativity, *Class. Quant. Grav.* **41**, 223001 (2024), [arXiv:2405.08868 \[gr-qc\]](#).
- [77] N. T. Bishop, R. Gomez, P. R. Holvorcem, R. A. Matzner, P. Papadopoulos, and J. Winicour, Cauchy-characteristic matching: A new approach to radiation boundary conditions, *Phys. Rev. Lett.* **76**, 4303 (1996).
- [78] M. R. Dubal, R. A. d’Inverno, and J. A. Vickers, Combining cauchy and characteristic codes. v. cauchy-characteristic matching for a spherical spacetime containing a perfect fluid, *Phys. Rev. D* **58**, 044019 (1998).
- [79] R. Gomez, P. Laguna, P. Papadopoulos, and J. Winicour, Cauchy characteristic evolution of Einstein-Klein-Gordon systems, *Phys. Rev. D* **54**, 4719 (1996), [arXiv:gr-qc/9603060](#).
- [80] C. J. S. Clarke, R. A. d’Inverno, and J. A. Vickers, Combining cauchy and characteristic codes. i. the vacuum cylindrically symmetric problem, *Phys. Rev. D* **52**, 6863 (1995).
- [81] M. R. Dubal, R. A. d’Inverno, and C. J. S. Clarke, Combining cauchy and characteristic codes. ii. the interface problem for vacuum cylindrical symmetry, *Phys. Rev. D* **52**, 6868 (1995).
- [82] R. A. d’Inverno, M. R. Dubal, and E. A. Sarkies, Cauchy characteristic matching for a family of cylindrical vacuum solutions possessing both gravitational degrees of freedom, *Class. Quant. Grav.* **17**, 3157 (2000), [arXiv:gr-qc/0002057](#).
- [83] R. A. d’Inverno and J. A. Vickers, Combining cauchy and characteristic codes. iii. the interface problem in axial symmetry, *Phys. Rev. D* **54**, 4919 (1996).
- [84] R. A. d’Inverno and J. A. Vickers, Combining cauchy and characteristic codes. iv. the characteristic field equations in axial symmetry, *Phys. Rev. D* **56**, 772 (1997).
- [85] A. M. Abrahams *et al.* (Binary Black Hole Grand Challenge Alliance), Gravitational wave extraction and outer boundary conditions by perturbative matching, *Phys. Rev. Lett.* **80**, 1812 (1998), [arXiv:gr-qc/9709082](#).
- [86] M. E. Rupright, A. M. Abrahams, and L. Rezzolla,

- Cauchy perturbative matching and outer boundary conditions. I. Methods and tests, *Phys. Rev. D* **58**, 044005 (1998), arXiv:gr-qc/9802011.
- [87] L. Rezzolla, A. M. Abrahams, R. A. Matzner, M. E. Rupright, and S. L. Shapiro, Cauchy perturbative matching and outer boundary conditions: Computational studies, *Phys. Rev. D* **59**, 064001 (1999), arXiv:gr-qc/9807047.
- [88] T. Giannakopoulos, *Characteristic formulations of general relativity and applications*, Other thesis (2023), arXiv:2308.16001 [gr-qc].
- [89] T. Giannakopoulos, D. Hilditch, and M. Zilhao, Hyperbolicity of General Relativity in Bondi-like gauges, *Phys. Rev. D* **102**, 064035 (2020), arXiv:2007.06419 [gr-qc].
- [90] T. Giannakopoulos, N. T. Bishop, D. Hilditch, D. Pollney, and M. Zilhao, Gauge structure of the Einstein field equations in Bondi-like coordinates, *Phys. Rev. D* **105**, 084055 (2022), arXiv:2111.14794 [gr-qc].
- [91] T. Giannakopoulos, N. T. Bishop, D. Hilditch, D. Pollney, and M. Zilhão, Numerical convergence of model Cauchy-characteristic extraction and matching, *Phys. Rev. D* **108**, 104033 (2023), arXiv:2306.13010 [gr-qc].
- [92] C. Gundlach, Simulations of gravitational collapse in null coordinates. III. Hyperbolicity, *Phys. Rev. D* **110**, 024020 (2024), arXiv:2404.16720 [gr-qc].
- [93] S. Ma *et al.*, Fully relativistic three-dimensional Cauchy-characteristic matching for physical degrees of freedom, *Phys. Rev. D* **109**, 124027 (2024), arXiv:2308.10361 [gr-qc].
- [94] R. H. Price, Nonspherical perturbations of relativistic gravitational collapse. i. scalar and gravitational perturbations, *Phys. Rev. D* **5**, 2419 (1972).
- [95] E. W. Leaver, Spectral decomposition of the perturbation response of the schwarzschild geometry, *Phys. Rev. D* **34**, 384 (1986).
- [96] K. S. Thorne and S. J. Kovacs, The generation of gravitational waves. I. Weak-field sources., *Astrophys. J.* **200**, 245 (1975).
- [97] K. S. Thorne, Multipole expansions of gravitational radiation, *Rev. Mod. Phys.* **52**, 299 (1980).
- [98] L. Blanchet and T. Damour, Tail-transported temporal correlations in the dynamics of a gravitating system, *Phys. Rev. D* **37**, 1410 (1988).
- [99] L. Lindblom, M. A. Scheel, L. E. Kidder, R. Owen, and O. Rinne, A New generalized harmonic evolution system, *Class. Quant. Grav.* **23**, S447 (2006), arXiv:gr-qc/0512093 [gr-qc].
- [100] L. E. Kidder, L. Lindblom, M. A. Scheel, L. T. Buchman, and H. P. Pfeiffer, Boundary conditions for the Einstein evolution system, *Phys. Rev. D* **71**, 064020 (2005), arXiv:gr-qc/0412116 [gr-qc].
- [101] L. T. Buchman and O. C. A. Sarbach, Towards absorbing outer boundaries in general relativity, *Class. Quant. Grav.* **23**, 6709 (2006), arXiv:gr-qc/0608051.
- [102] L. T. Buchman and O. C. A. Sarbach, Improved outer boundary conditions for Einstein's field equations, *Class. Quant. Grav.* **24**, S307 (2007), arXiv:gr-qc/0703129.
- [103] O. Rinne, L. T. Buchman, M. A. Scheel, and H. P. Pfeiffer, Implementation of higher-order absorbing boundary conditions for the Einstein equations, *Class. Quant. Grav.* **26**, 075009 (2009), arXiv:0811.3593 [gr-qc].
- [104] L. T. Buchman, M. D. Duez, M. Morales, M. A. Scheel, T. M. Kosterlitz, A. M. Evans, and K. Mitman, Numerical relativity multimodal waveforms using absorbing boundary conditions, *Class. Quant. Grav.* **41**, 175011 (2024), arXiv:2402.12544 [gr-qc].
- [105] O. Rinne, Stable radiation-controlling boundary conditions for the generalized harmonic Einstein equations, *Class. Quant. Grav.* **23**, 6275 (2006), arXiv:gr-qc/0606053 [gr-qc].
- [106] O. Rinne, L. Lindblom, and M. A. Scheel, Testing outer boundary treatments for the Einstein equations, *Class. Quant. Grav.* **24**, 4053 (2007), arXiv:0704.0782 [gr-qc].
- [107] C. Dailey, E. Schnetter, and N. Afshordi, Formulating the complete initial boundary value problem in numerical relativity to model black hole echoes, *Class. Quant. Grav.* **42**, 025002 (2025), arXiv:2409.17970 [gr-qc].
- [108] B. Szilagy, L. Lindblom, and M. A. Scheel, Simulations of Binary Black Hole Mergers Using Spectral Methods, *Phys. Rev. D* **80**, 124010 (2009), arXiv:0909.3557 [gr-qc].
- [109] D. Sun, S. Ma, M. A. Scheel, and S. Teukolsky, Gauge boundary conditions to mitigate com drift in bbh simulations, in preparation.
- [110] H. Bondi, M. G. J. van der Burg, and A. W. K. Metzner, Gravitational Waves in General Relativity. VII. Waves from Axi-Symmetric Isolated Systems, *Proceedings of the Royal Society of London Series A* **269**, 21 (1962).
- [111] R. K. Sachs, Gravitational waves in general relativity viii. waves in asymptotically flat space-time, *Proceedings of the Royal Society of London. Series A. Mathematical and Physical Sciences* **270**, 103 (1962).
- [112] B. Szilagy, J. Blackman, A. Buonanno, A. Taracchini, H. P. Pfeiffer, M. A. Scheel, T. Chu, L. E. Kidder, and Y. Pan, Approaching the Post-Newtonian Regime with Numerical Relativity: A Compact-Object Binary Simulation Spanning 350 Gravitational-Wave Cycles, *Phys. Rev. Lett.* **115**, 031102 (2015), arXiv:1502.04953 [gr-qc].
- [113] N. Deppe, W. Throwe, L. E. Kidder, N. L. Vu, K. C. Nelli, *et al.*, *Spectre*, 10.5281/zenodo.10967177 (2024).
- [114] The Spectral Einstein Code, <http://www.black-holes.org/SpEC.html>.
- [115] G. Lovelace *et al.*, Simulating binary black hole mergers using discontinuous Galerkin methods, *Class. Quant. Grav.* **42**, 035001 (2025), arXiv:2410.00265 [gr-qc].
- [116] B. Szilagy, Key Elements of Robustness in Binary Black Hole Evolutions using Spectral Methods, *Int. J. Mod. Phys. D* **23**, 1430014 (2014), arXiv:1405.3693 [gr-qc].
- [117] J. W. York, Jr., Conformal 'thin sandwich' data for the initial-value problem, *Phys. Rev. Lett.* **82**, 1350 (1999), arXiv:gr-qc/9810051 [gr-qc].
- [118] H. P. Pfeiffer and J. W. York, Jr., Extrinsic curvature and the Einstein constraints, *Phys. Rev. D* **67**, 044022 (2003), arXiv:gr-qc/0207095 [gr-qc].
- [119] H. P. Pfeiffer, The Initial value problem in numerical relativity, *J. Hyperbol. Diff. Equat.* **2**, 497 (2005), arXiv:gr-qc/0412002.
- [120] V. Varma, M. A. Scheel, and H. P. Pfeiffer, Comparison of binary black hole initial data sets, *Phys. Rev. D* **98**, 104011 (2018), arXiv:1808.08228 [gr-qc].
- [121] M. Boyle, Transformations of asymptotic gravitational-wave data, *Phys. Rev. D* **93**, 084031 (2016), arXiv:1509.00862 [gr-qc].
- [122] M. De Amicis *et al.*, Late-time tails in nonlinear evolutions of merging black holes, (2024), arXiv:2412.06887 [gr-qc].
- [123] A. Ashtekar, T. De Lorenzo, and N. Khera, Compact binary coalescences: Constraints on waveforms, *Gen. Rel. Grav.* **52**, 107 (2020), arXiv:1906.00913 [gr-qc].

- [124] D. A. B. Iozzo, M. Boyle, N. Deppe, J. Moxon, M. A. Scheel, L. E. Kidder, H. P. Pfeiffer, and S. A. Teukolsky, Extending gravitational wave extraction using Weyl characteristic fields, *Phys. Rev. D* **103**, 024039 (2021), [arXiv:2010.15200 \[gr-qc\]](#).
- [125] H. P. Pfeiffer, D. A. Brown, L. E. Kidder, L. Lindblom, G. Lovelace, and M. A. Scheel, Reducing orbital eccentricity in binary black hole simulations, *New frontiers in numerical relativity. Proceedings, International Meeting, NFNR 2006, Potsdam, Germany, July 17-21, 2006*, *Class. Quant. Grav.* **24**, S59 (2007), [arXiv:gr-qc/0702106 \[gr-qc\]](#).
- [126] A. Buonanno, L. E. Kidder, A. H. Mroue, H. P. Pfeiffer, and A. Taracchini, Reducing orbital eccentricity of precessing black-hole binaries, *Phys. Rev.* **D83**, 104034 (2011), [arXiv:1012.1549 \[gr-qc\]](#).
- [127] A. H. Mroue and H. P. Pfeiffer, Precessing Binary Black Holes Simulations: Quasicircular Initial Data, (2012), [arXiv:1210.2958 \[gr-qc\]](#).
- [128] S. Ma, K. Mitman, L. Sun, N. Deppe, F. Hébert, L. E. Kidder, J. Moxon, W. Throwe, N. L. Vu, and Y. Chen, Quasinormal-mode filters: A new approach to analyze the gravitational-wave ringdown of binary black-hole mergers, *Phys. Rev. D* **106**, 084036 (2022), [arXiv:2207.10870 \[gr-qc\]](#).
- [129] S. Ma, L. Sun, and Y. Chen, Black Hole Spectroscopy by Mode Cleaning, *Phys. Rev. Lett.* **130**, 141401 (2023), [arXiv:2301.06705 \[gr-qc\]](#).
- [130] S. Ma, L. Sun, and Y. Chen, Using rational filters to uncover the first ringdown overtone in GW150914, *Phys. Rev. D* **107**, 084010 (2023), [arXiv:2301.06639 \[gr-qc\]](#).
- [131] https://github.com/Sizheng-Ma/qnm_filter.
- [132] T. May, S. Ma, J. L. Ripley, and W. E. East, Nonlinear effect of absorption on the ringdown of a spinning black hole, *Phys. Rev. D* **110**, 084034 (2024), [arXiv:2405.18303 \[gr-qc\]](#).
- [133] N. Khera, S. Ma, and H. Yang, Quadratic Mode Couplings in Rotating Black Holes and Their Detectability, (2024), [arXiv:2410.14529 \[gr-qc\]](#).
- [134] D. P. O’Leary and B. W. Rust, Variable projection for nonlinear least squares problems, *Computational Optimization and Applications* **54**, 579 (2013).
- [135] M. Giesler *et al.*, Overtones and Nonlinearities in Binary Black Hole Ringdowns, (2024), [arXiv:2411.11269 \[gr-qc\]](#).
- [136] M. De Amicis, S. Albanesi, and G. Carullo, Inspiral-inherited ringdown tails, *Phys. Rev. D* **110**, 104005 (2024), [arXiv:2406.17018 \[gr-qc\]](#).
- [137] V. Cardoso, G. Carullo, M. De Amicis, F. Duque, T. Katagiri, D. Pereniguez, J. Redondo-Yuste, T. F. M. Spieksma, and Z. Zhong, Hushing black holes: Tails in dynamical spacetimes, *Phys. Rev. D* **109**, L121502 (2024), [arXiv:2405.12290 \[gr-qc\]](#).
- [138] S. Okuzumi, K. Ioka, and M.-a. Sakagami, Possible Discovery of Nonlinear Tail and Quasinormal Modes in Black Hole Ringdown, *Phys. Rev. D* **77**, 124018 (2008), [arXiv:0803.0501 \[gr-qc\]](#).
- [139] S. R. Green, F. Carrasco, and L. Lehner, Holographic Path to the Turbulent Side of Gravity, *Phys. Rev. X* **4**, 011001 (2014), [arXiv:1309.7940 \[hep-th\]](#).
- [140] H. Yang, A. Zimmerman, A. Zenginoglu, F. Zhang, E. Berti, and Y. Chen, Quasinormal modes of nearly extremal Kerr spacetimes: spectrum bifurcation and power-law ringdown, *Phys. Rev. D* **88**, 044047 (2013), [arXiv:1307.8086 \[gr-qc\]](#).
- [141] S. Ma and H. Yang, Excitation of quadratic quasinormal modes for Kerr black holes, *Phys. Rev. D* **109**, 104070 (2024), [arXiv:2401.15516 \[gr-qc\]](#).
- [142] S. Albanesi, S. Bernuzzi, T. Damour, A. Nagar, and A. Placidi, Faithful effective-one-body waveform of small-mass-ratio coalescing black hole binaries: The eccentric, nonspinning case, *Phys. Rev. D* **108**, 084037 (2023), [arXiv:2305.19336 \[gr-qc\]](#).
- [143] T. Islam, G. Faggioli, G. Khanna, S. E. Field, M. van de Meent, and A. Buonanno, Phenomenology and origin of late-time tails in eccentric binary black hole mergers, (2024), [arXiv:2407.04682 \[gr-qc\]](#).
- [144] B. Szilagyi and J. Winicour, Well posed initial boundary evolution in general relativity, *Phys. Rev. D* **68**, 041501 (2003), [arXiv:gr-qc/0205044](#).
- [145] https://spectre-code.org/structCce_1_1InitializeJ_1_1ConformalFactor.html.
- [146] N. Bishop, D. Pollney, and C. Reisswig, Initial data transients in binary black hole evolutions, *Class. Quant. Grav.* **28**, 155019 (2011), [arXiv:1101.5492 \[gr-qc\]](#).
- [147] E. E. Flanagan and D. A. Nichols, Conserved charges of the extended Bondi-Metzner-Sachs algebra, *Phys. Rev. D* **95**, 044002 (2017), [Erratum: *Phys.Rev.D* 108, 069902 (2023)], [arXiv:1510.03386 \[hep-th\]](#).